Space Sci Rev (2007) 129: 245–278
DOI 10.1007/s11214-007-9176-4

Planetary Magnetic Fields and Solar Forcing: Implications for Atmospheric Evolution

Rickard Lundin · Helmut Lammer · Ignasi Ribas

Received: 4 April 2006 / Accepted: 22 March 2007 /
Published online: 3 July 2007

Abstract The solar wind and the solar XUV/EUV radiation constitute a permanent forcing of the upper atmosphere of the planets in our solar system, thereby affecting the habitability and chances for life to emerge on a planet. The forcing is essentially inversely proportional to the square of the distance to the Sun and, therefore, is most important for the innermost planets in our solar system—the Earth-like planets. The effect of these two forcing terms is to ionize, heat, chemically modify, and slowly erode the upper atmosphere throughout the lifetime of a planet. The closer to the Sun, the more efficient are these process. Atmospheric erosion is due to thermal and non-thermal escape. Gravity constitutes the major protection mechanism for thermal escape, while the non-thermal escape caused by the ionizing X-rays and EUV radiation and the solar wind require other means of protection. Ionospheric plasma energization and ion pickup represent two categories of non-thermal escape processes that may bring matter up to high velocities, well beyond escape velocity. These energization processes have now been studied by a number of plasma instruments orbiting Earth, Mars, and Venus for decades. Plasma measurement results therefore constitute the most useful empirical data basis for the subject under discussion. This does not imply that ionospheric plasma energization and ion pickup are the main processes for the atmospheric escape, but they remain processes that can be most easily tested against empirical data.

Shielding the upper atmosphere of a planet against solar XUV, EUV, and solar wind forcing requires strong gravity and a strong intrinsic dipole magnetic field. For instance, the strong dipole magnetic field of the Earth provides a "magnetic umbrella", fending of the solar wind at a distance of 10 Earth radii. Conversely, the lack of a strong intrinsic magnetic field at Mars and Venus means that the solar wind has more direct access to their topside

R. Lundin (✉)
Swedish Institute of Space Physics (IRF), Box 812, 98128 Kiruna, Sweden
e-mail: rickard@irf.se

H. Lammer
Space Research Institute, Austrian Academy of Sciences, Schmiedlstr. 6, 8042 Graz, Austria

I. Ribas
Facultat de Ciències, Campus UAB, Institut de Ciències des l'Espai (CSIC-IEEC), Torre C5-parellE, 08193 Bellaterra, Spain

atmosphere, the reason that Mars and Venus, planets lacking strong intrinsic magnetic fields, have so much less water than the Earth?

Climatologic and atmospheric loss process over evolutionary timescales of planetary atmospheres can only be understood if one considers the fact that the radiation and plasma environment of the Sun has changed substantially with time. Standard stellar evolutionary models indicate that the Sun after its arrival at the Zero-Age Main Sequence (ZAMS) 4.5 Gyr ago had a total luminosity of ≈70% of the present Sun. This should have led to a much cooler Earth in the past, while geological and fossil evidence indicate otherwise. In addition, observations by various satellites and studies of solar proxies (Sun-like stars with different age) indicate that the young Sun was rotating more than 10 times its present rate and had correspondingly strong dynamo-driven high-energy emissions which resulted in strong X-ray and extreme ultraviolet (XUV) emissions, up to several 100 times stronger than the present Sun. Further, evidence of a much denser early solar wind and the mass loss rate of the young Sun can be determined from collision of ionized stellar winds of the solar proxies, with the partially ionized gas in the interstellar medium. Empirical correlations of stellar mass loss rates with X-ray surface flux values allows one to estimate the solar wind mass flux at earlier times, when the solar wind may have been more than 1000 times more massive.

The main conclusions drawn on basis of the Sun-in-time-, and a time-dependent model of plasma energization/escape is that:

1. Solar forcing is effective in removing volatiles, primarily water, from planets,
2. planets orbiting close to the early Sun were subject to a heavy loss of water, the effect being most profound for Venus and Mars, and
3. a persistent planetary magnetic field, like the Earth's dipole field, provides a shield against solar wind scavenging.

Keywords Planetary magnetospheres · Solar forcing · Young Sun · Ionospheric plasma escape · Loss of planetary water

1 Introduction

Solar forcing affects the planets in the inner solar system in different ways, the most obvious being the solar gravitation force. But there are also other forcing terms affecting the planets: solar irradiation and the solar plasma outflow. The solar irradiation, with a spectrum from X-ray to infrared, provides the highest input power to the planetary environment, corresponding to a power between 490–720 W/m^2 for Mars, with its elliptic orbit, for the Earth 1370 W/m^2, and 2620 W/m^2 for Venus. The power input from solar plasma outflow/the solar wind, is quite variable, but the average power is six orders of magnitude smaller (0.001–0.003 W/m^2). Yet, one may argue that the solar plasma forcing has a more significant effect on a planetary atmosphere than solar irradiation alone. For instance, thermal escape (due to solar irradiation) primarily favours light atoms and molecules (e.g. hydrogen) while non-thermal escape processes (due to solar plasma forcing) are much less mass sensitive. Nonthermal escape in general results in an order of magnitude higher mass loss for the Earth-like planets. This apparent anomaly, with orders of magnitude difference in input power, demonstrates the non-linear behaviour of nature, i.e. sheer power is not sufficient to explain physical phenomena. It is the process that matters, such as in this case for the escape of planetary volatiles.

Thermal escape from an atmosphere is determined from a Maxwellian (thermalized) particle distribution, the escape rate given by the temperature of the distribution at the exobase and the escape velocity of the object at the exobase. Theoretically all particles within the Maxwellian distribution of particles having velocities above the escape velocity will be lost. *Nonthermal escape* may be defined as all other processes where the energization and escape of particles is related with (microscopic) nonthermal processes. Excluded are all (macroscopic) processes of catastrophic nature such as e.g. impact erosion by in falling objects from space. Non-thermal escape is not unrelated to thermal escape, because most non-thermal escape processes are based on the existence of photo ionization processes. The electromagnetic radiation from the Sun also determines the scale-height of the atmosphere, and correspondingly also the ionosphere and cross-sectional area for e.g. solar wind forcing. However, we separate the two mechanisms mainly because of their differences with respect to solar forcing. Thermal escape is (mainly) due to solar radiation, whereas non-thermal escape is related with a broader aspect of solar wind forcing, such as sputtering, ion pickup, ionospheric plasma energization etc. The basic argument is that solar wind energy and momentum, electromagnetic or corpuscular, defines the forcing regardless of individual processes inferred. Following the definitions by Chassefière et al. (2007), there are two classes of thermal escape:

1. Jeans escape, driven by EUV and XUV heating of the upper atmosphere. Atmospheric atoms having velocities above escape velocity at the exobase level are free to escape into space.
2. Hydrodynamic escape, consisting of a bulk expansion of the upper atmosphere due to intense solar EUV/XUV fluxes, allowing atoms to overcome the gravitational binding force. Hydrodynamic escape plays an important role in low gravity environments (e.g. comets), but is also considered to have played a major role in outflow during early Noachian on Mars (e.g. Chassefière and Leblanc 2004).

With regard to non-thermal escape we present a slightly modified definition as compared to that proposed by Chassefière et al. (2007). The following four processes here identify non-thermal escape:

1. Photochemical escape, associated with dissociative recombination. Ions produced by photo ionization may reach higher temperatures than the neutral atmosphere in the ionosphere. Recombination/charge-exchange produce energetic neutrals, some of them have sufficient velocity to escape the planet (e.g. Luhmann et al. 1992; Lammer et al. 1996; Fox and Hac 1997; Kim et al. 1998; Chassefière and Leblanc 2004).
2. Ion sputtering produced by ions impacting the upper atmosphere/corona leads to the ejection of neutral particles (e.g. Luhmann et al. 1992; Jakosky et al. 1994; Johnson et al. 2000; Leblanc and Johnson 2002).
3. Ionospheric plasma energization and escape driven by direct solar wind forcing (e.g. Pérez-de Tejada 1987, 1998; Lundin and Dubinin 1992). The process is more complex for a planet with an intrinsic magnetic dynamo such as the Earth (see e.g. Moore et al. 1999, for a review). Plasma waves are important for the transfer of energy and momentum from the solar wind to planetary magnetospheres (see e.g. Chaston et al. 2005). In a similar manner, waves observed in the shocked solar wind plasma are likely to take part in the energization of ionospheric ions near Mars (e.g. Espley et al. 2004; Winningham et al. 2006; Lundin et al. 2006b).
4. Ionospheric ion pickup, a process caused by the protrusion of the solar wind motional electric field into a planetary ionosphere. The combined solar wind electric and magnetic

field ($\underline{E} \times \underline{B}$) results in a cycloid motion of energized ionospheric ions (Luhmann and Kozyra 1991; Dubinin et al. 1993; Kallio et al. 1998; Kallio and Janhunen 2002; Ma et al. 2004; Nagy et al. 2004; Kallio et al. 2006; Dubinin et al. 2006; Luhmann et al. 2006). Mass loading leads to a local weakening of the motional electric field, and a correspondingly lower energization (Lundin et al. 1991; Kallio et al. 1998).

Notice that the first two non-thermal escape processes are associated with the escape of neutral atoms, while the last two processes are associated with the energization and escape of ionospheric plasma. In what follows we will focus on the energization and escape of ionospheric plasma. One important reason for this, obvious from the title of this report, is that a planetary magnetic field has implications for the ionospheric plasma escape and the corresponding atmospheric evolution. Another important reason is that ionospheric plasma escape is a topic where theory may be compared with numerous direct in situ observations. Photochemical escape and sputtering are processes that by and large lack adequate in situ measurements. Studies of the latter two processes are therefore based on models and simulations. In a similar way, quantitative results of thermal escape (Jeans escape and hydrodynamic escape) are based on models and simulations.

The magnetic field plays an important role in controlling ionized gases—plasmas. The solar wind, a wind of plasma escaping from the Sun, is in fact embedded in (frozen-in) the solar magnetic field (Alfvén 1950; Parker 1958). In the same manner a plasma flow, like the solar wind, cannot easily protrude into a strong planetary magnetic field. For instance, the Earth's dipole magnetic field acts as a "magnetic umbrella" fending off the solar wind (Fig. 1). The standoff distance from the Earth is typically some 70 000 km away in the sub solar region. Conversely, planets lacking strong intrinsic magnetic fields such as Mars and Venus have no "magnetic umbrella", and the solar wind can directly access the upper atmosphere. Recent measurements from Mars (Lundin et al. 2004b) show that the solar wind may impact as low as 270 km above the dayside surface of Mars. This illustrates the problem for planetary atmospheres without magnetic shielding. The relative erosion rate of ionospheric plasma is consequently lower for the Earth than for Mars, for example. The total outflow rate for the Earth, the mass flux dominated by O^+ ions, is 1–3 kg/s (Chappell et al. 1987). However, recent data and arguments suggest that most of the outflowing ions

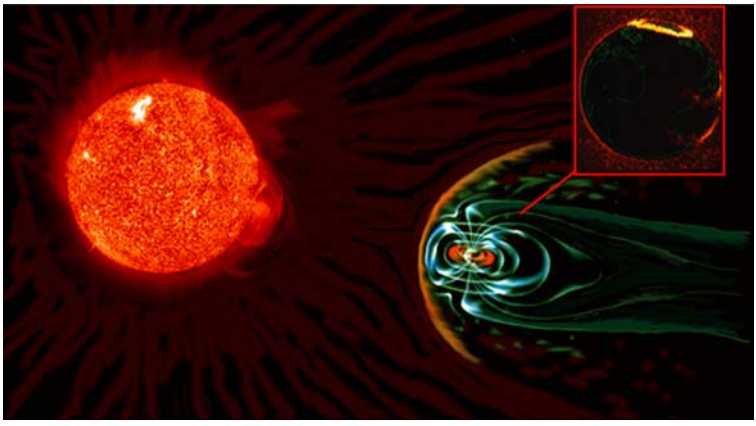

Fig. 1 The magnetic field of the Earth acting as a shield against direct solar wind forcing of the Earths atmosphere and ionosphere. The aurora in the close-up view of the Earth (*upper right*) illustrates that a limited amount of solar wind forcing occurs in the polar region

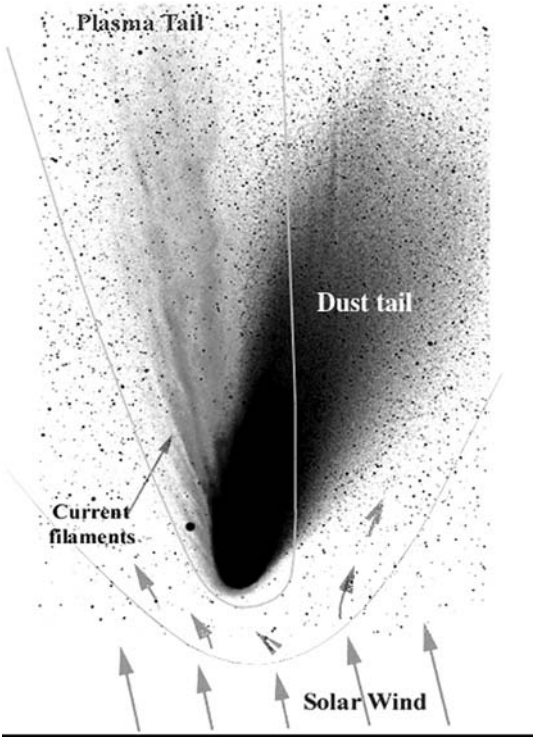

Fig. 2 The comet tail, an example of direct forcing by the Sun, the solar EUV/UV and the solar wind

are recaptured by the Earth (Seki et al. 2001), i.e. less than 1 kg/s are lost to space. For Mars, the mass loss of O^+ and O_2^+ during solar maximum has been estimated to be $\approx$1 kg/s (Lundin et al. 1989). Recent data from Mars Express imply a much lower escape during solar minimum (Barabash et al. 2007), with orders of magnitude variability connected with solar wind dynamic pressure changes (Lundin et al. 2006b). Mars has a very tenuous atmosphere, the average atmospheric pressure being two orders of magnitude lower than on the Earth. Moreover, the area of the solar wind obstacle (the solid planet) is about four times larger for the Earth compared to Mars. Therefore, considering the volatile inventory on both planets, Mars is losing atmospheric O^+ and O_2^+ much faster compared to the Earth.

Weakly magnetized planets like Mars and Venus, behave like comets, the nightside cavities forming elongated tails of escaping planetary plasma originating from the upper atmosphere/ionosphere. The planetary wind is stretching out in the antisolar direction in the same way as for comets (Fig. 2) yet at a rate lower than for a typical comet during solar approach. The main difference between a planet and a comet in terms of volatile escape is mass/gravity. Venus and Mars have much stronger gravity, which retains volatile substances for billions of years before they are significantly eroded away by the solar wind. The low gravity of comets means that their atmosphere builds up and expands while approaching the Sun, leading to a gradually expanding obstacle for the erosive solar wind. The loss from a km-size comet (e.g. Halley) is $1–10\times10^6$ kg/day at 1 AU, while the loss from the Venus and Mars is typically 100 times lower. The heavy loss of matter is a reason why the tails of comets are visible and the plasma tails of planets are not.

The present rate of escape observed from a weakly magnetized planet such as Mars corresponds to significant losses of volatiles throughout the planetary lifetime. For instance,

Lammer et al. (1996, 2003) and Lundin and Barabash (2004a) estimated the loss of volatiles during the last 3.5 billion years; the water loss corresponds to a global equivalent layer GEL of 10–30 meters. These figures were obtained by considering the evolution of the Sun (Wood et al. 2002) and of the planetary atmosphere. On the other hand, morphological surface features suggest that more surface and near-surface water was present during Noachian and Hesperian times (GEL 100–500 m) (McKay and Stoker 1989; Baker 2001; Lunine et al. 2003; Bibring et al. 2004; Neukum 2005; Bertaux et al., this volume; Nisbet et al., this volume). In a similar manner Venus may have been subject to a heavy loss of water (Kulikov et al. 2006, 2007). The interaction of the solar wind with Venus (Russell et al. 2006) and the corresponding rate of outflow by ion pickup processes (Luhmann and Bauer 1992; Luhmann et al. 2006) based on Pioneer Venus Orbiter PVO measurements suggest a modest solar wind interaction with Venus. On the other hand, the comet-like ionospheric features found by Brace et al. (1987) imply a rather strong ionospheric response to solar forcing.

Under the assumption that all Earth-like planets accreted from matter of essentially the same chemical origin, the differences we observe today may be related with evolutionary processes. The evolution of volatiles is one particular aspect of that. The Earth is the only planet where a significant hydrosphere remains, while Mars and particularly Venus are strongly dehydrated in comparison.

In this report we discuss the evolution of planetary volatiles, with a focus on water, under varying solar forcing conditions with time. Our focus is on the acceleration and escape of ionospheric plasma, for reasons already mentioned, but also because we believe that plasma escape to a large extent couples to the other escape processes. We start by describing the variability of the solar radiation and the solar plasma environment. We continue by defining and describing the internal forcing that leads to the solar output and the external forcing that the Sun imposes on the planets. We then discuss why magnetic shielding plays such an important role in protecting a planetary atmosphere. Finally, we present a model and a scenario of the loss of water and CO_2 from Mars, Venus and the Earth. We conclude on basis of this that a strong intrinsic magnetic field is important for maintaining water on a planet. A wealth of water is central for the evolution of life, for making a planet habitable for more advanced life-forms.

2 Variability of the Solar Radiation and Plasma Environment

The Sun is the main source of surface and atmosphere energy for the Earth-like planets, interior energy/heat flow playing a negligible role. Without a dependable (stable) star like the Sun, the Earth would not have developed a rich and diverse biosphere, the home to millions of living species. This raises two questions: Why only on the Earth, and not also on Mars and Venus? Has the Sun always been "dependable"? We focus in this section on the second question, addressing in the following continuing sections an issue related with a biosphere on the Earth-like planets—the water inventory.

2.1 Short-Time Solar Variability

High precision radiometric observations of the Sun carried out by several satellites since the late Seventies have shown that the Sun undergoes small cyclic variations in brightness. These brightness changes are closely related with the ≈11-year sunspot cycle. Lean (1997) found that the observed bolometric luminosity of the Sun varied over the recent solar cycles 21, 22, and 23 (from about 1978) by about 0.12%.

The Sun is brightest during the times of maximum sunspot numbers and faintest during the sunspot minima. This can be explained by the larger changes in the area coverage and intensity of magnetic white light facular regions that peak near sunspot maximum. The observed light variations of the Sun arise from the blocking effect of sunspots and increased facular contribution to brightness, which slightly offsets the former. Even though the observed light bolometric variations of the Sun are very small over its activity cycle, variations over the sunspot cycle are much larger at shorter wavelengths (e.g., Lean 1997; Guinan and Ribas 2002).

For example, typical variations of solar coronal X-ray emissions from the minimum to the maximum of the ≈11-year activity cycle are ≈500% (Guinan and Ribas 2002). The cyclic changes arising from variations in the chromospheres and transition region emission range from 10–200% at NUV, FUV and EUV wavelengths. Also the frequencies and intensities of flaring events and coronal mass ejections (CME) are strongly correlated with the Sun's activity cycle. For example, the rate of CME occurrences is larger during the sunspot maxima than during sunspot minima (Webb and Howard 1994).

These cyclic short-time variations play a role in Earth's global climate, and numerous studies have been carried out on the possible influence of the 11-year solar cycle on climate, frequency of storms and cyclones, rainfall, droughts, vegetation, insect populations, etc. (see, e.g., Hoyt and Schatten 1997).

However, Earth's expected cyclic temperature variation of about 0.1°C at the surface, computed from simple black body considerations and the small change of irradiance of 0.12%, does not seem sufficient in itself to produce observable climate changes (e.g. Foukal et al. 2006). On the other hand, the changes in the XUV flux of the Sun over a typical activity cycle are significantly larger that the total irradiance changes, and these high energy solar emissions are absorbed, heating the Earth's stratosphere and thermosphere. Although the deposited energy is small, non-linear feedback mechanisms could amplify the affects on climate by altering, for example, the tropospheric heat exchange between the equator and the polar regions.

An interesting and surprisingly close connection between the solar cycle effects and the climate presented by Friis-Christensen and Lassen (1991) has been a matter of controversy for some time. The finding was followed by an equally surprisingly good connection between cloud cover and cosmic radiation (Svensmark and Friis-Christensen 1997; Svensmark 2000; Kanipe 2006). The authors argue that certain clouds are formed as a result of the precipitation of galactic cosmic ray particles. Since the solar magnetic field and the solar wind acts as a shield and damper for galactic cosmic ray particles, the variability of the solar magnetic field will modulate the cosmic ray flux in the inner part of the solar system. In this way the solar activity, and the corresponding generation/escape of solar magnetic flux may represent a climate controller for the Earth-like planets. Very recently Svensmark et al. (2006) showed results from a laboratory experiment that may very well be the final proof for the hypothesis of cloud formation by cosmic ray fluxes.

2.2 Temporal Variation of the Sun's Total Luminosity

Because of ever accelerating nuclear reactions in its core, the Sun is a slowly evolving variable star that has undergone a ≈30% increase in luminosity over the past 4.5 Gyr. Solar evolution models show that in ≈1 Gyr from now, when the Sun is about 10% brighter, the Earth will be heated enough so that its oceans start to evaporate. About 6 Gyr from now the Sun expands beyond the Earth orbit to become a red giant.

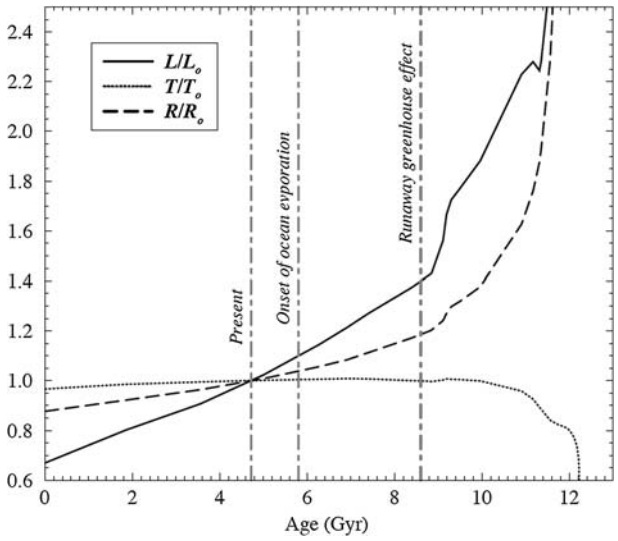

Fig. 3 The evolution of the effective temperature, radius, and luminosity of the Sun from the zero-age main sequence (ZAMS) to the start of its red giant phase. The *vertical lines* mark the approximate expected occurrences of Earth-related phenomena such as the onset of ocean evaporation and the start of the runaway greenhouse effect. Based on the evolution models of Bressan et al. (1993) and the predictions by Kasting (1988)

The nuclear evolution of the Sun is generally well understood from stellar evolutionary theory. We also have a good understanding of the internal solar structure thanks to helioseismology, although the former excellent agreement between observation and theory has been disturbed by recent updates in the abundances of some key elements (Guzik et al. 2006). For example, models for the ZAMS Sun given by Bressan et al. (1993) indicate values of $L = 0.67 L_{\mathrm{Sun}}$, $R = 0.89 R_{\mathrm{Sun}}$, and $T_{\mathrm{eff}} = 0.96 T_{\mathrm{eff\,Sun}}$ (where $T_{\mathrm{eff\,Sun}} = 5777$ K). A plot showing the evolution of the luminosity, radius, and temperature of the Sun according to Bressan et al. (1993) is shown in Fig. 3.

One finds from these standard stellar evolutionary models that the young Sun, about 4.6 Gyr ago, was ≈200 K cooler and ≈10% smaller than today and had an initial luminosity of ≈70% of the present Sun so that in the early stages of the Solar System, the young Sun's irradiance (Solar constant) is expected to have been significantly lower. The lower luminosity of the young Sun should have lead to a much cooler Earth in the past. However, paleoclimate studies show that the young Earth always had liquid water and was, therefore, typically warmer (possibly heated by greenhouse gases such as CO_2 and CH_4), than during recent times. The increase in solar luminosity over the history of geologic time periods and its effect on the Earth's climate have been discussed by various authors in the past (e.g., Sagan and Mullen 1972; Newman and Rood 1977; Owen 1979). On the other hand, a young Sun with a slightly higher initial solar mass than previously assumed would produce a slightly higher total luminosity (Kasting et al. 1993; Whitmire et al. 1995; Sackmann and Boothroyd 2003) and could also be a viable explanation for warm temperatures on early Earth and Mars, otherwise are difficult to account for, in particularly for Mars. Sackmann and Boothroyd (2003) pointed out that such a higher initial solar mass leaves a fingerprint on the Sun's present internal structure that is large enough to be detectable, in principle, via helioseismic observations. Their computations demonstrated that several mass-losing solar models are more consistent with the helioseismic observations than is the standard solar model (Sackmann and Boothroyd 2003). However, there are several uncertainties in the observed solar composition and in the input physics on which solar models are based and these uncertainties have a slightly larger effect on the Sun's present internal structure than a possible fingerprint left from an early efficient solar mass loss. Future improvements by a

factor of 2 in the accuracy of input parameters for solar mass loss models could reduce the size of the uncertainties below the level of the fingerprints left by a more massive, brighter young Sun. This would allow us to determine whether early solar mass loss took place or not. More observations of mass loss rates from other young solar-like stars similar to the young Sun are needed.

The impact of the solar radiation and particle fluxes on the evolution of planetary atmospheres and their water inventories has received much less attention than studies of the climate change and greenhouse effect. Previous observation-based studies have indicated that the young Sun was a far stronger source of energetic particles and electromagnetic radiation (e.g., Newkirk 1980; Zahnle and Walker 1982; Ayres 1997; Güdel et al. 1997) than today's Sun. These early studies are now supported by a large number of multiwavelength (X-ray, EUV, FUV, UV, optical) observations of solar proxies providing solid evidence that the early Sun was a much more active star than it is at present (e.g., Ribas et al. 2005).

2.3 Evolution of Solar X-Rays and EUV Radiation

Because ionization, thermospheric heating, production of extended neutral gas corona, and thermal and non-thermal escape of atmospheric constituents all depend on the evolution of the solar X-ray and EUV radiation (XUV) and the solar wind, one cannot neglect the changing solar radiation and plasma environment in the study of the evolution of planetary atmospheres. The relevant wavelengths for the heating of upper atmospheres of planets are the ionizing ones $\lambda \leq 102.7$ nm (e.g., Gordiets et al. 1982; Hunten 1993; Bauer and Lammer 2004), which contain only a small fraction of the present solar spectral power. The high radiation levels of the young Sun were triggered by strong magnetic activity. The magnetic activity of the Sun is expected to have greatly decreased with time (Skumanich 1972; Simon et al. 1985; Güdel et al. 1997; Guinan and Ribas 2002; Ribas et al. 2005) as the solar rotation slowed down through angular momentum loss. Observational evidence and theoretical models suggest that the young Sun rotated about 10 times faster than today and had significantly enhanced magnetically generated coronal and chromospheric activity (Keppens et al. 1995; Guinan and Ribas 2002; Ribas et al. 2005).

The NASA sponsored "Sun in Time" program (Dorren and Guinan 1994) was established to study the magnetic evolution of the Sun using a homogeneous sample of single nearby G0-V main sequence stars which have known rotation periods and well-determined physical properties, including temperatures, metal abundances and ages that cover most of the Sun's main sequence lifetime from 130 Myr to 8.5 Gyr. The observations, obtained with various satellites like ASCA, ROSAT, EUVE, FUSE and IUE satellites, cover a range between 0.1- and 330 nm, except for a gap at between 36–92 nm, which is a region of very strong interstellar medium absorption. Details of the datasets and the flux calibration procedure employed are provided in Ribas et al. (2005). The results indicate that the young main sequence Sun was about 100–1000 times stronger in XUV emissions than at present. Similarly, the transition region and chromospheric FUV–UV emissions of the young Sun are expected to be 10–100 and 5–10 times stronger, respectively, than at present, and the flux variation over age is therefore a steep wavelength function. Figure 4 shows the time evolution of the spectral range with 0.1 nm $< l <$ 100 nm, which includes X-rays and EUV and the *Lyman-α* line at 121.56 nm (Lammer et al. 2003; Ribas et al. 2005) at a distance of 1 AU.

In the 100–0.1 nm interval, the fluxes follow a power-law relationship $I_{\mathrm{XUV}}(t)/I_{\mathrm{XUV}} = 6.16 \cdot (t[\mathrm{Gyr}]^{-1.19})$. At longer wavelengths, the *Lyman-α* emission feature can contribute to a significant fraction of the XUV flux. High-resolution *Hubble Space Telescope* (HST)

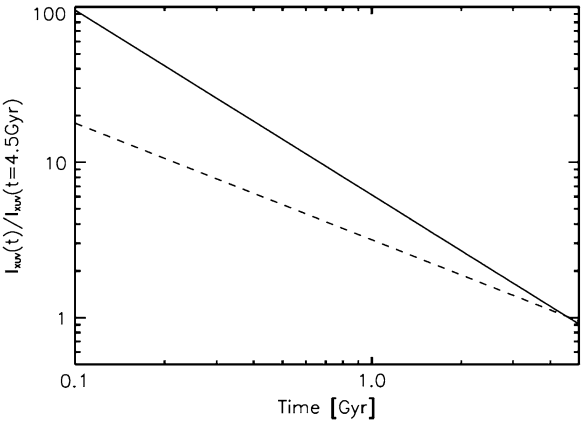

Fig. 4 Time evolution of the I_{XUV} energy flux for solar-like G stars (*solid line*: $\lambda = 100$–0.1 nm; *dashed line*: *Lyman-α* $= 121.56$ nm) (Ribas et al. 2005)

spectroscopic observations were used to estimate the net stellar flux. These measurements, together with the observed solar *Lyman-α* define the following power-law relationship with high correlation $I_{\mathrm{L}\alpha}(t)I_{\mathrm{L}\alpha} = 3.17 \cdot (t[\mathrm{Gyr}])^{-0.75}$.

In both power-laws, the XUV and *Lyman-α* expressions are valid for ages between 0.1–7 Gyr, I_{XUV} and $I_{\mathrm{L}\alpha}$ are the present integrated fluxes at 1 AU and $I_{\mathrm{XUV}}(t)$ and $I_{\mathrm{L}\alpha}(t)$ are the integrated fluxes as a function of time. One finds fluxes of $\approx 6 \cdot I_{\mathrm{XUV}}$ and $\approx 3 \cdot I_{\mathrm{L}\alpha}$ about 3.5 Gyr ago, and $\approx 100 \cdot I_{\mathrm{XUV}}$ and $\approx 20 \cdot I_{\mathrm{L}\alpha}$ about 100 Myr after the Sun arrived on the ZAMS.

2.4 The Solar Wind of the Young Sun

HST high-resolution spectroscopic observations of the H *Lyman-α* feature of several nearby main-sequence G and K stars carried out by Wood et al. (2002) have revealed neutral hydrogen absorption associated with the interaction between the stars' fully ionized coronal winds with the partially ionized local interstellar medium. Wood et al. (2002) modelled the absorption features formed in the astrospheres of these stars and provided the first empirically estimated coronal mass loss rates for solar-like G and K main sequence stars. They estimated the mass loss rates from the system geometry and hydrodynamics and found from their small sample of G and K-type stars, where astrospheres which can be observed, that mass loss rates increase with stellar activity. This study suggests that the young Sun had a much more dense solar wind than today. The correlation between mass loss and X-ray surface flux follows a power law relationship, which indicates an average solar wind density up to 1000 times higher than today during the first 100 Myr after the Sun reached the ZAMS.

Mass loss rates of cool, main sequence stars depend on their rotation periods, which are in turn correlated with the stars' ages. To obtain the evolution of the stellar wind velocity v_{sw} and stellar wind density n_{sw} of solar-like stars, one can use the X-ray activity-stellar mass loss and solar wind velocity power-law relations of Wood et al. (2002) and Newkirk (1980). One obtains the time-behaviour of the solar wind parameters (Griemeier et al. 2004) $v_{\mathrm{sw}} = v^*[1 + (t/\tau)]^{-0.4}$ and particle density $n_{\mathrm{sw}} = n^*[1 + (t/\tau)]^{-1.5}$.

The proportionality constants are determined by average present-day solar wind conditions (Griemeier et al. 2004). With $v_{\mathrm{sw}} = 400\ \mathrm{km\,s^{-1}}$ and $n_{\mathrm{sw}} = 10^7\ \mathrm{m^{-3}}$ for $t = 4.6$ Gyr and at $d = 1$ AU (Schwenn 1990) one obtains $v^* = 3200\ \mathrm{km\,s^{-1}}$, $n^* = 2.4 \cdot 10^{10}\ \mathrm{m^{-3}}$ (density at 1 AU). The time constant is $\tau = 2.56 \cdot 10^7$ yr (Newkirk 1980). For distances other than 1 AU, the solar wind parameters can be scaled with an r^{-2} dependency. The time variation of $n(t)$ at Earth orbit of 1 AU is shown in Fig. 5. One can see from Fig. 5 that the observational

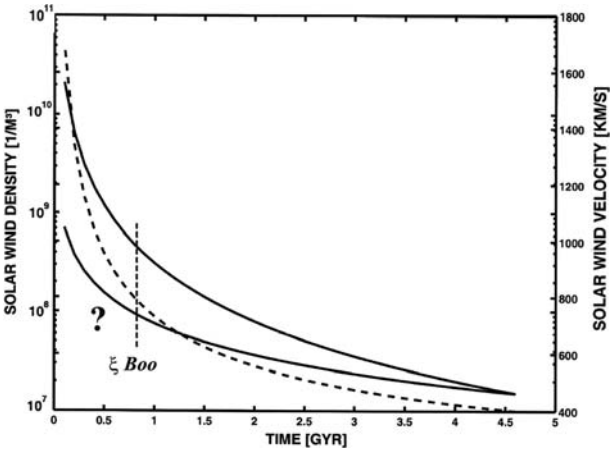

Fig. 5 Evolution of the observational based minimum and maximum stellar wind densities scaled to 1 AU (*left scale: solid lines*) obtained from several nearby solar-like stars. On the *right scale* one can see the evolution of the stellar wind velocity (*dashed curve*). More observations or early active stars with ages less than 700 Myr are needed to obtain a better picture of the mass-loss/activity relation shortly after the Sun arrived at the ZAMS

data for solar-like G and K stars suggest that more active stars have higher mass loss rates and solar wind number density. However, observations of the active M dwarf star *Proxima Cen* and the active *RS CVn* system λ *And* (G8 IV + M V) are inconsistent with this relation and show lower mass loss rates. A recent observation of the solar-like young star ξ *Boo* also shows a lower mass loss rate, consistent with the mass loss rates previously found for *Proxima Cen* and λ *And* (Wood et al. 2005).

The common feature of these three stars is that they are all very active in X-ray surface fluxes at about 10^6 erg cm^{-2} s^{-1}, about a factor of 30 larger than the Sun and corresponding to a time of about 700 Myr after solar-like stars arrived at the ZAMS. The results of these observations show the uncertainty of early mass loss and solar wind estimations, because ξ *Boo* is a usual but very active young solar-like star, while *Proxima Cen* and λ *And* are different types than normal G and K stars. One can speculate that there may be a high-activity cut-off to the mass-loss/activity relation obtained by Wood et al. (2002), although more active young solar-like G and K stars with X-ray surface fluxes larger than 10^6 erg cm^{-2} s^{-1} should be observed and studied in the future.

3 External and Internal Forcing

3.1 The Solar Output—Internal Forcing

Internal forcing is here defined as forcing emanating from the body itself—from internal energy sources. The solar output (the solar irradiance and the solar corpuscular radiation) is an example of internal forcing. Also the variability of the internal forcing as discussed in Sect. 2 is driven by the interior of the Sun, or at least dominated by internal processes. However, one cannot completely rule out the possibility of external influences on the solar output. An example of this is Jupiter, where internal forcing matches, or even exceeds external (solar wind) forcing. Numerous examples may also be found in astrophysics, such as binary stars.

As mentioned in Sect. 2.2, the solar luminosity is expected to vary little with time, on a long—as well as short term base. However, solar X-rays and EUV, changing orders of magnitude on longer-terms, are also subject to a high short-term variability. Radiation in this frequency range represents the most variable part of the solar irradiance. Equally, or even

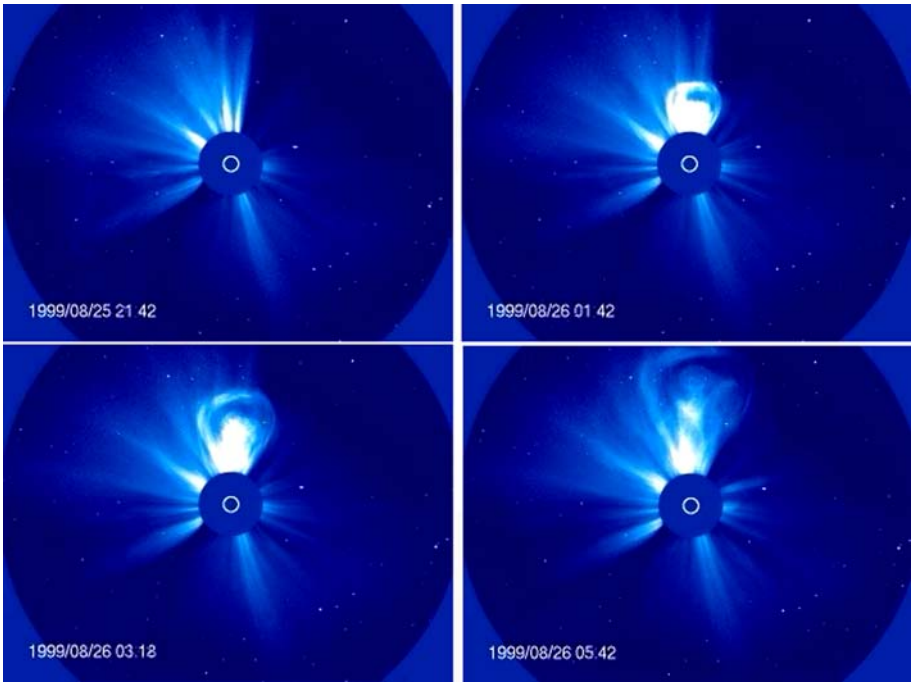

Fig. 6 SOHO/LASCO image of a time sequence showing the variable outflow of solar coronal plasma, characterized by streamers and a CME

more variable, is the coronal plasma escape, the solar wind and solar energetic particles. This is demonstrated by the SOHO image of the solar corona (Fig. 6). The coronal outflow displays a strong and dynamic variation in space and time. The structured coronal plasma escape may vary by several orders of magnitude, especially during solar maximum—the most active period of the solar cycle. This is also the time of maximum X-ray and EUV flux. The difference in coronal plasma escape and X-ray, EUV fluxes, is substantial between solar maximum and solar minimum. For instance, the solar wind dynamic pressure reaches about an order of magnitude higher during solar maximum compared to solar minimum, and the occurrence frequency of CMEs increases by a factor of five or more (e.g. Bird and Edenhofer 1990, and references therein). Similarly, solar EUV fluxes are a factor 2–4 higher during solar maximum compared to solar minimum.

The connection between internal processes, the solar irradiance, the coronal mass escape, and their relation to the solar variability is beyond the scope of this report. Various aspects connected with internal forcing are discussed in Sect. 2. We simply conclude here that solar internal forcing results in variable and structured phenomena undergoing short-term ($\approx$11, 22, 80, 200, 1000, ... year, Lundstedt et al. 2006) cyclic variations as well as long-term ($\approx$100–4600 million years) changes (e.g.Wood et al. 2002, 2005, and Ribas et al. 2005)

3.2 External Forcing—Direct and Indirect

External forcing of a celestial object exposed to the solar wind may be categorized into two groups, *direct forcing* and *indirect forcing*. By direct forcing we mean that the solar wind has direct access to the obstacle, whereby energy and momentum can be transferred locally.

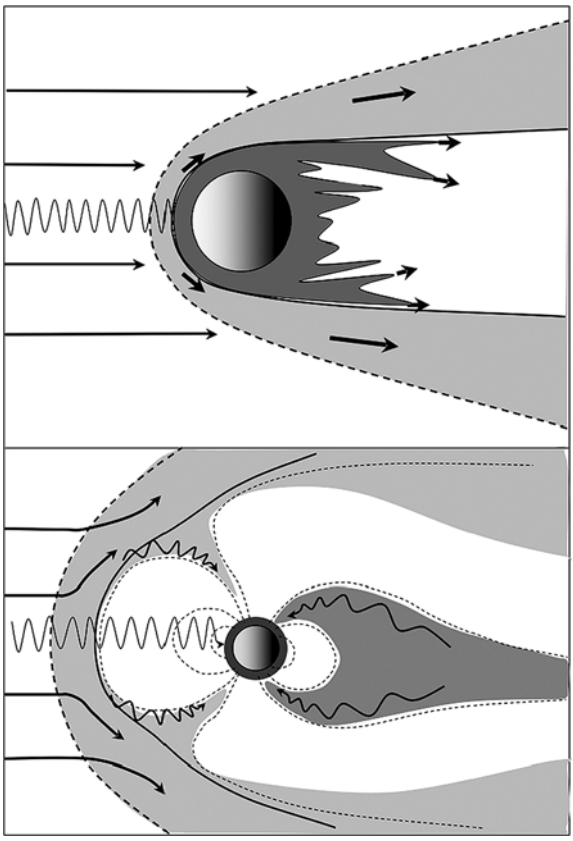

Fig. 7 Diagram illustrating the two types of external forcing, direct forcing (*upper*) and indirect forcing (*bottom*). In the latter case the atmosphere/ionosphere is protected by a strong intrinsic magnetic field

Conversely, indirect forcing implies that there is no direct contact. Energy and momentum may yet be transferred/mediated to the obstacle by other means such as waves, electric fields and electric currents. Figure 7 illustrates these two categories of solar wind forcing. In the bottom figure a magnetic field acts as a shield against direct plasma forcing (indirect forcing dominates). Direct forcing, (direct contact between the planetary ionosphere/atmosphere and solar wind plasma) may also occur for a strongly magnetized planet like the Earth, but then only in narrow dayside "cusp" regions, as indicated in Fig. 7.

A comet approaching the Sun illustrates direct forcing. A low gravity and the lack of a protective "shield" means that a comet is subject to massive forcing by solar radiation and the solar wind. The solar radiation heats the surface, leading to a release of particles/gas constituting the coma. The solar EUV may lead to such a high degree of ionization, the $N_e/N_{neutral}$ ratio exceeding 10^{-6}, that electric and magnetic fields become the dominating forcing terms in the local gas dynamics. The picture of comet Hale-Bop (Fig. 2) illustrates this quite well. Notice that a comet of the Hale-Bop composition and size has two tails—a high-speed plasma tail induced by the solar wind interaction pointing away from the Sun (less the aberration) and—a dust tail comprising debris along the comet trajectory. The plasma tail is a cometary wind consisting of ionized matter/gas from the comet—plasma and energized neutrals. The cometary wind gradually reaches solar wind velocities in the deep tail (≈300–900 km/s). Such high velocities as compared to the comet orbital velocity (tens of km/s) represent a complete loss, i.e. the particles have no chance to return to the

comet. The "rays" observed in the dust tail, suggests that the solar wind may remove also large parts of the dust tail.

Indirect forcing may occur also for shielded/protected objects. In this case the forcing may be considered a "leakage" through the shield, but it may also be considered a global process that couples to external conditions in the solar wind. Magnetic reconnection (Dungey 1961) is an example of a global coupling between an external magnetic field and the internal magnetic field of a celestial object. For suitable boundary conditions this may lead to indirect external forcing. A dense, re-radiating, atmosphere may also serve as a shield for solar irradiation, while only a strong dipole magnetic field is capable of protecting the atmosphere/ ionosphere from fast charged particles.

3.3 Magnetic Shielding

Global magnetic shielding is well known from space plasma- and cosmic ray physics. Magnetic shielding is governed by the Lorenz-force, prohibiting incident charged particles from protruding deeper than two Larmor radii perpendicular to the local magnetic field (**B**). The exception is when an electric field (**E**) is applied perpendicular to the magnetic field, i.e. $\mathbf{F} = e\mathbf{E} + e[\mathbf{v} \times \mathbf{B}]$, and charged particles may protrude/convect across the magnetic field. In reality the physics is more complex, with second order forcing terms contributing, and particles may traverse deeper than two Larmor radii. Nevertheless, a sufficiently strong magnetic field acts as a stopper, a magnetic shield, fending off charged particles and prohibiting them from accessing deep regions of a magnetic field domain. Figures 1 and 7 (lower) illustrate how magnetic shielding deflects the solar wind. Energy and momentum may yet cross the stopping boundary by various processes (magnetic reconnection, diffusion, viscous interaction, Kelvin–Helmholtz instabilities, impulsive penetration, see e.g. (Keyser et al. 2005) for a review) and propagate along magnetic field lines to the ionosphere/atmosphere.

The magnetized celestial object best known to us is the Earth. The strong terrestrial magnetic dipole serves as an excellent shield, fending off the solar wind at about 10 Earth radii (Re) in the solar direction. A "bubble", *a magnetosphere*, is created, separating the solar wind plasma from the near Earth environment (Fig. 1). The terrestrial magnetosphere exemplifies the indirect forcing. The transfer of solar wind energy and momentum across the dayside-stopping boundary, the magnetopause, provide essentially all plasma forcing of the Earth's ionosphere and atmosphere by indirect means. Penetrating plasma energy and momentum are converted in a dynamo to electric fields, currents and waves that subsequently propagate down, leading to forcing in the ionosphere and upper atmosphere.

Global magnetic shielding is therefore not sufficient to prohibit external plasma forcing. However, a strong magnetic dipole field markedly reduces the efficiency of energy and momentum transfer; the stronger the intrinsic dipole field, the lower the efficiency of external forcing.

Without magnetic shielding by an intrinsic magnetic dipole (e.g. Venus and Mars) the atmosphere and ionosphere are directly exposed to the solar wind, leading to a more direct solar wind forcing. The combined EUV and solar wind forcing lead to ionization and efficient removal of atmospheric atoms and molecules from the topside atmosphere. On the other hand the solar wind ram pressure transmitted to the ionosphere of Mars and Venus induces a magnetic barrier (e.g. Zhang et al. 1991, and Crider et al. 2004), sometimes referred to as a solar wind magnetic field pile-up. This induced magnetic barrier also serves as a magnetic shield such that the solar wind is swept sideways along the flanks as illustrated in Fig. 7. However, the magnetic barrier is not a solid obstacle. The upper ionosphere is in direct contact with shocked solar wind plasma; the motional solar wind electric field,

waves and protruding solar wind ions allow energy and momentum transfer to the topside ionosphere. In the next section we describe how solar wind energy and momentum is transferred to planetary ions as a result of direct forcing.

3.4 Energy and Momentum Transfer

The solar wind interaction with the unprotected upper atmosphere and ionosphere of a planet results in a transfer of energy and momentum to planetary particles. A number of processes may be conceived, but the removal of matter boils down to kinetics. The available energy and momentum of the solar wind limit the total outflow by all non-thermal escape processes. Here we do not discuss irradiative solar forcing (ponderomotive forcing) as an energy and momentum transfer process. Radiative forcing is associated with heating and ionization of a planetary atmosphere, indirectly responsible for thermal (Jeans, hydrodynamic) escape and dissociated recombination. In what follows we focus on the two ionospheric plasma escape processes related with non-thermal escape.

The efficiency of non-thermal escape is related to the energy and momentum transfer efficiency and the cross-sectional area exposed to the solar wind. A low gravity and lack of a magnetic shield imply an extended atmosphere and a larger cross-sectional area for direct solar wind scavenging. Besides solar X-rays and EUV ionization other ionization processes, such as electron impact ionization (Zhang et al. 1993), take place in the exosphere of non-magnetized planets. These ionization processes lead to further heating of the upper atmosphere, enhanced ionization and increased transfer of energy and momentum to the ionosphere and exosphere.

The transfer of energy and momentum by the solar wind takes place in the topside atmosphere and ionosphere, where the solar wind may interact with ionospheric plasma and neutral gas. Interaction with ionospheric plasma leads to energization and escape, as described in the Introduction. Solar wind interaction with neutral gas may lead to further ionization from electron impact and to ion sputtering and the ejection of neutral particles (see Introduction). The interaction region lies within the altitude range above the planet where the transfer of solar wind energy and momentum takes place. A simple fluid dynamic description of the interaction region above a non-magnetized planet is described in Fig. 8. Two cross section areas, A_{M} and A_{max}, are marked out within the interaction volume that stretches out along the tail. Interaction (i.e., transfer of solar wind energy and momentum to the planetary plasma embedded in the flow) is expected to continue until balance in momentum flux is achieved between the solar- and planetary tail plasma. The cross section areas in Fig. 8 are selected because they have been experimentally determined, For instance, Lundin and Dubinin (1992), used A_{M} ($A_{\mathrm{M}} = \pi(R_{\mathrm{o}}^2 - R_{\mathrm{i}}^2)$) as the minimum cross-sectional area to estimate the theoretical escape from Mars. They used R_{o} as the altitude of experimentally determined "mass loading boundary" and R_{i} as the unperturbed/cold Martian ionosphere, as a minimum cross section of the interaction volume along the flanks. The interaction volume expands towards the tail, the tailward flaring leading to the other cross-section area extreme $A_{\mathrm{max}} = \pi R_{\mathrm{Tail}}^2$. Assuming a symmetric distribution of the solar wind and planetary wind through the flow channels determined by A_{M} and A_{max}, we may compare model outflow with experimental data.

The solar wind energy and momentum transfer responsible for the energization and loss of matter from, for example the upper Martian atmosphere and ionosphere has been estimated based on fairly straightforward considerations (Pérez-de Tejada 1987, 1998; Lundin

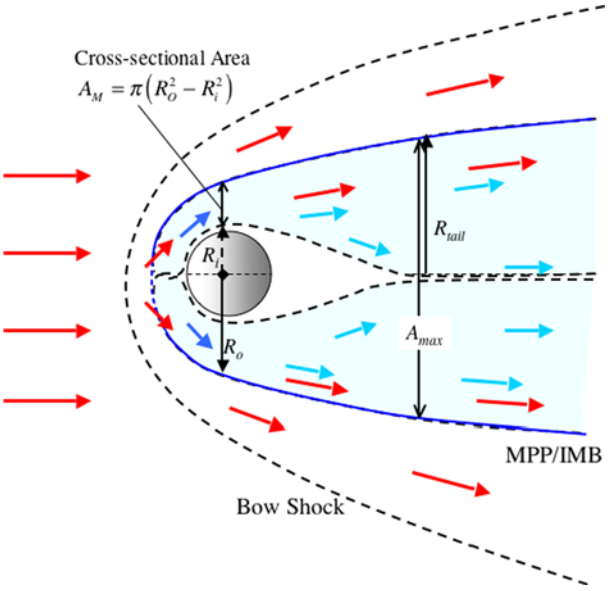

Fig. 8 Diagram of solar wind plasma forcing of a non-magnetized planetary atmosphere/ionosphere. The cross-sectional area and depth constitute the region of solar wind energy and momentum transfer. *Blue arrows* illustrate planetary ion escape. Notice that energy and momentum transfer (by solar wind motional electric field, waves, etc.) is expected to occur within the flow volume extending from the subsolar region to the deep tail

and Dubinin 1992). From the conservation of energy and momentum in the transfer of energy and momentum flux for the solar wind (Φ_{SW}) and Martian ions (Φ_M) one may obtain:

$$\Phi_M = \frac{v_{SW} \cdot m_{SW}}{v_M \cdot m_M}\left(\Phi_{SW} - \frac{v_{i,SW}}{v_{SW}}\Phi_{i,SW}\right) \cdot \frac{\delta_{SW}}{\delta_M}, \tag{1}$$

where $\Phi_{i,SW}$ and, $v_{i,SW}$ is the local/decelerated solar wind flux and velocity respectively. The ratio δ_{SW}/δ_M defines the relative momentum exchange thickness, here assumed to be $\approx$1. The above equation illustrates that the Martian ion flux is strongly coupled to speed (v_M) and mass (m_M) of the outflowing ions. The ratio between the solar wind velocity and the planetary ions v_{SW}/v_M, provides a flux amplification for ions of equal masses. This means that slowly escaping ions lead to higher mass losses. As illustrated in Fig. 9, the maximum escape flux for a solar wind velocity of 400 km/s may be amplified by up to 80 times the solar wind flux in the Martian environment ($v_{esc} = 5$ km/s), and by a factor of 5 if the escaping ions have 16 times higher mass than the solar wind protons. Thus, due to the high solar wind velocity and the relatively low escape velocity, a very high escape rate is theoretically feasible for Mars.

The net escaping mass flux from a planet subject to direct solar wind forcing, S_M, may now be obtained from:

$$S_M = A \cdot m_M \cdot \Phi_M \text{ (kg/s)}, \tag{2}$$

where Φ_M is the ion outflow of mass m_M, and A is the cross-sectional area ($A_M \rightarrow A_{max}$).

Lundin and Dubinin (1992) made a simple estimate of the input versus output mass flux on Mars by comparing measurement data with average solar wind input. The estimated range of cross-sectional areas $A_M \approx 1.6 \times 10^{14}$ and $A_{max} = 6.5 \times 10^{14}$ m^2 were based on measurement data of the planetary heavy ion escape (e.g. O^+). Using a solar wind proton density and velocity of 5×10^6 m^{-3} and 400 km/s respectively, the total solar wind flux through the cross-sectional is $\Phi_{SW} = 2 \times 10^{12}$ (m^{-2} s^{-1}). The corresponding range of solar wind mass flux input then corresponds to 0.53 kg/s and 2.2 kg/s respectively. This is in the

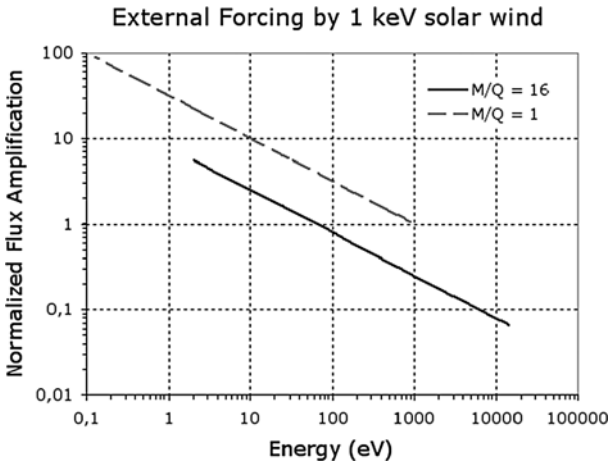

Fig. 9 Normalized momentum exchange by external solar wind forcing, illustrating the amplification of escape flux with decreasing outflow velocity (1)

range of Martian ion escape observed (Lundin et al. 1989), i.e. ≈1 kg/s. However, considering the amplification factor (Fig. 9) the escape mass flux may be much higher for low outflow velocities. If for instance O^+ ions are escaping at a velocity of 10 km/s (≈8.4 eV), about twice the escape velocity at Mars, a typical solar wind energy and momentum transfer would lead to a theoretical O^+ outflow in the range 6–25 kg/s.

4 Solar Radiative and Particle Forcing of the Earth-Like Planets

The distance to the Sun matters for both the irradiance and the solar wind forcing. For the two extremes, Venus and Mars, the unit radiative and particle forcing differs by a factor of ≈4. Despite this, the differences in the present solar forcing are relatively small. Moreover, the difference in atmospheric composition and density is less obvious when studying the ionospheres of the Earth-like planets. The ionization by solar EUV leads to classical Chapman layers, largely similar in electron density and ion composition, the highest ion abundance being O_2^+ in the lower ionosphere and O^+ in the upper ionosphere. The corresponding mass outflow/escape from the Earth-like planets are therefore likely to be dominated by the above constituents. This is certainly the case for the Earth (e.g. Chappell et al. 1987) and Mars (Lundin et al. 1989; Carlsson et al. 2006), and apparently also for Venus (Lundin et al. 2007). It raises the question about the molecular source of oxygen, water or CO_2? No doubt the Earth's outflow of H^+ and O^+ originates from water, but what about Venus and Mars, both planets having atmospheres dominated by CO_2? We will return to this in a forthcoming section.

Table 1 illustrates the power input by solar radiation and particles.

The solar wind input power for the Earth is obtained by assuming a limited (1–2%) transfer of energy through the magnetopause. An interesting and important aspect of the input power is the six order of magnitude difference between solar power of the solar irradiation and the solar wind power. The difference intuitively suggests that solar irradiation is the main driver for ionospheric and atmospheric processes. This is certainly the case for heating/expansion and dayside ionization of the atmosphere. However, this difference is not the case for the outflow/escape of matter. As already noted in Sect. 1, accelerated ionospheric O^+ dominates the escaping mass flux from the Earth. As indicated by the title of this report, our focus is on the implications of a planetary magnetic field for solar forcing. Our

Table 1 Solar input power to the Earth-like planets

	Solar irradiation power (W)	Solar wind input on the "obstacle" (W)
Venus	3.1×10^{17}	1.6×10^{11}
Earth	1.8×10^{17}	2.6×10^{11}
Mars	2.2×10^{16}	1.1×10^{11}

escape model is based on empirical data of ionospheric plasma escape, demonstrating that plasma escape is expected to be more severe for non-magnetized planets. This does not rule out other processes such as e.g. hydrodynamic escape (Chassefière and Leblanc 2004) and dissociated recombination (Luhmann et al. 1992). On the contrary, adding all processes together suggests an even more dramatic past for non-magnetized planets in the inner solar system.

5 The Present Loss of Volatiles from the Earth-Like Planets

The volatile content, abundances and states of the Earth-like planets, remains an intriguing issue in planetology. Consider the following alternative theories:

(1) the present differences in volatile content of the planets is directly related to the accretion process, or
(2) the present differences in volatile content is a consequence of the long-term evolution of the planets (gain/loss).

The first theory assumes an initial accretion differentiation of the planets. The second theory suggests long-term evolutionary differentiation of the planetary volatile content.

Considering the overall similarities such as proximity to the Sun and average density, it seems reasonable to assume that the Earth-like planets aggregated from the same matter in the early solar nebula under rather similar conditions. Earth and Mars apparently acquired significant hydrospheres, indicating that the same may have occurred on Venus. The issue therefore appears to be—why did Mars, Venus and Earth evolve so differently? The distance to the Sun is an important factor, but it can hardly explain the present vast differences in atmospheric and hydrospheric conditions.

If evolutionary differentiation is the main cause, the following questions may be raised: by what mechanisms, when and how quickly? Catastrophic impact by large celestial objects in the early phase of the solar system is an obvious, yet circumstantial mechanism. The Earth was subject to such a bombardment, but it was also able to retain a vast hydrosphere and a dense atmosphere. Dynamical escape by solar forcing appears to be the most likely process responsible for a gradual depletion of the atmosphere and hydrosphere of the Earth-like planets. As discussed in Sects. 1–3, solar forcing leads to two types of escape processes—thermal escape and non-thermal escape.

Thermal escape is a process that favours light atoms. Thermal expansion and heating of a multispecies planetary atmosphere implies highest scale-height for light atoms, and therefore preference to escape (e.g. McElroy et al. 1977; Lewis and Prinn 1984; Pepin 1994). Hydrodynamic escape (Chassefière 1996) should be effective at Mars during an early/wet period (first ≈500 My) of intensified solar UV/EUV/XUV radiation. As will be demonstrated in this section such an expansion will also increase the cross-sectional area for the solar EUV/XUV, and solar wind forcing, the subsequent ionization leading to strong

non-thermal escape (dissociated recombination, sputtering, ionospheric plasma acceleration, and ion pickup) as described in Sect. 1. In this way thermal expansion and non-thermal escape are strongly coupled. Furthermore, as already demonstrated, ionospheric plasma energization and escape processes (Lundin and Dubinin 1992; Luhmann and Bauer 1992; Jakosky et al. 1994; Lammer et al. 1996, 2003) are more powerful in bringing large mass fluxes up to well beyond escape velocities, thus contributing to dehydrating unprotected bodies in the inner solar system. Before substantiating this further we consider the present volatile inventory on Earth, Venus and Mars (see e.g. Chassefière et al. 2007), where our focus is on the H_2O and CO_2 inventory.

Earth

The present volatile inventory according to Lewis and Prinn (1984) is 1.67×10^{21} kg H_2O, 9.2×10^{19} kg CO_2, and 4.3×10^{18} kg N_2 The Earth's total volatile mass is therefore 1.76×10^{21} kg, corresponding to ≈ 345 Bar. Note that there is an uncertainty related with the volatile content of CO_2 in rocks. The Earth is geologically active and plate tectonics makes estimates based on rock inventories difficult.

Mars

The present volatile inventory on Mars can be estimated by taking an average atmospheric pressure of 0.007 bars, mainly CO_2, with an admixture of N_2 (2.7%), and Ar (1.6%), for example. The atmospheric water content is highly variable but is generally less than 0.1%. Considering a surface area of 1.5×10^{14} m^2 we obtain a total atmospheric mass of $\approx 1.0 \times 10^{16}$ kg. The remaining volatile content, such as water, remains a matter of discussion (e.g. Carr and Head 2003; Bibring et al. 2004). Using a global equivalent layer (GEL) of water equal to 20 m, based estimates of the amount of water in the polar cap (Zuber et al. 1988) we obtain $\approx 3 \times 10^{18}$ kg H_2O. Assuming the same ratio between water and CO_2 on Mars as for the Earth ($\approx 6\%$) we obtain $\approx 2 \times 10^{17}$ kg CO_2, the latter assumed to be in the form of CO_2—ice in the south polar region and/or potentially in subsurface minerals, gas, and ice.

Venus

The volatile inventory in the mantle is unknown on Venus, so we can only rely on the volatile inventory in the atmosphere. The present volatile inventory in the Venus 90 bar atmosphere, essentially all CO_2, is according to Lewis and Prinn (1984): 4.1×10^{20} kg CO_2, with N_2 coming second in terms of abundance (1.6×10^{19} kg). The H_2O content amounts to $\approx 10^{16}$ kg. The total current water inventory on Venus is therefore some five orders of magnitude lower than that of the Earth.

Comparing Earth and Venus we note that Venus has more CO_2 and N_2 than the Earth, while the Earth has a higher total volatile inventory than Venus. Therefore, lacking a plausible chemical separation mechanism during the formation of the planetary atmospheres—favouring water on the Mars and CO_2 on Venus, one may hypothesize that the early Venus had a similar water inventory to the Earth. The question is therefore why the present Martian and Venusian volatile inventories are so different from the Earth.

On the other hand, if Venus had the same initial global water inventory as the Earth, with all water subsequently removed at a constant rate, the average loss rate would be about 10 000 kg/s. Recently Kulikov et al. (2006, 2007) studied how much of the H_2O-related oxygen could have been lost to space by the ion pick up process due to the stronger solar

wind and higher XUV fluxes of the young Sun and found, depending on the used solar wind parameters, that ion pick up by a strong early solar wind on a non-magnetized Venus could erode during 4.6 Gyr more than about 250 bar of atomic oxygen ions, corresponding to an equivalent amount of one terrestrial ocean. However, until we have better empiric data available on the ionospheric and atmospheric outflow from Venus we are left with just speculations.

5.1 Atmospheric Loss from Earth

The present outflow of atmospheric oxygen/hydrogen/nitrogen by nonthermal escape from the Earth is 1–3 kg/s (e.g. Chappell et al. 1987). The outflow is highly dependent on solar activity, varying on longer time scales between solar maximum and solar minimum, but also strongly on shorter times scales (CMEs, flare, etc., e.g. Moore et al. 1999). The outflow is induced by indirect forcing as previously discussed, the forcing mapping down to the auroral ionosphere guided by the Earth's dipole magnetic field (Fig. 10). If the outflow were considered as a loss at 3 kg/s and if that constituted N_2 and O_2, it would take about 50 billion years to evacuate the atmosphere. The corresponding time to deplete the ocean would be about 15 000 billion years. The margin for the present Earth is therefore comfortingly high. Furthermore, because of the strong Terrestrial magnetic dipole field, a recycling of outflowing planetary ions takes place (e.g. Seki et al. 2001). A conservative estimate of the total atmospheric loss is about 1 kg/s or less for the Earth.

Figure 11 demonstrates the variability of the average ionospheric plasma escape (for solar minimum and solar maximum), the right-hand side showing that the O^+/H^+ ratio corresponds to an erosion of plasma from above $\approx$1000 km during solar minimum. Solar cycle dependence is also evident since O^+ ions dominate during solar maximum. The latter implies a higher mass flux as well; more mass is "lost" during solar maximum. There are two main reasons for the enhanced O^+ outflow: (1) increased scale height from enhanced X-ray and EUV fluxes, and (2) enhanced solar wind plasma forcing. As will be discussed later, these are also the two prime reasons for the long-term erosion of planetary volatiles. Notice that the escape of nitrogen is omitted. Nitrogen escape as N^+ and N_2^+ is generally low compared to O^+ escape. The N^+/O^+ escape ratio reported (e.g. Yau and Whalen 1991; Yau et al. 1993) is of the order $\approx$0.1, implying that the loss of volatiles from the Earth by nonthermal escape primarily originates from water.

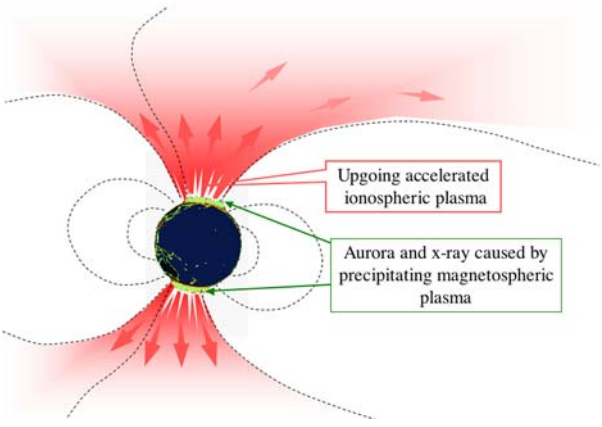

Fig. 10 Effects of external forcing on a magnetized object like the Earth, causing polar aurora and polar region plasma outflow

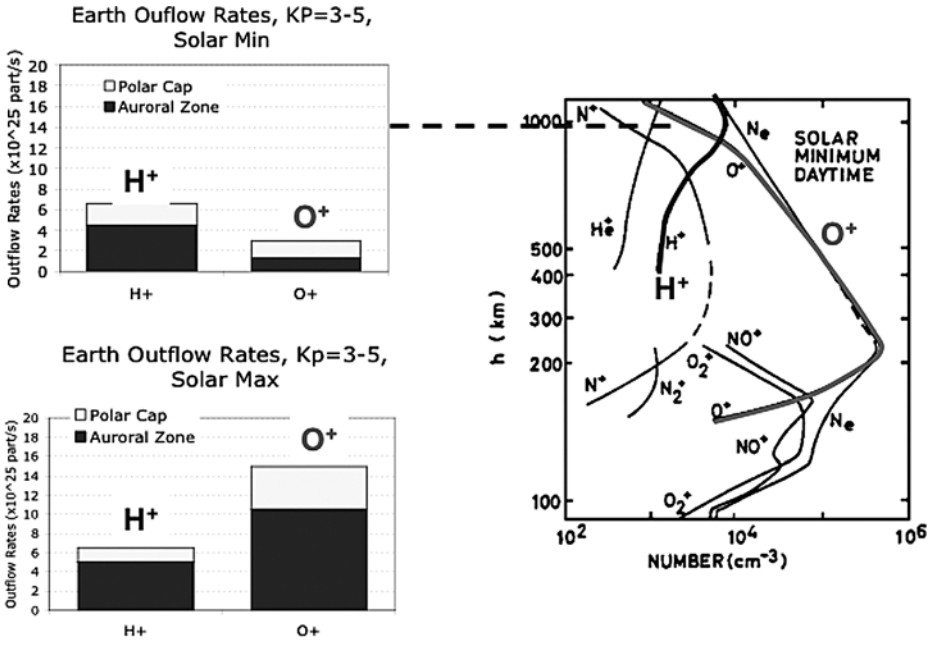

Fig. 11 *Left*: Solar minimum/maximum and ionospheric plasma outflow rate (Yau and Whalen 1991; Yau et al. 1993). *Right*: Solar minimum ionospheric ion profile illustrating that the outflow during solar minimum corresponds to an equivalent altitude of 1,000 km

5.2 Atmospheric Loss from Present MARS—Phobos-2, Mars Express

Phobos-2, launched in July 1988, was the first spacecraft enabling a quantitative estimate of the volatile escape form Mars. Based on the energized outflow of H^+, O^+, O_2^+ and CO_2^+ detected by the ASPERA experiment on Phobos-2 (Lundin et al. 1989) it was possible to estimate the volatile loss from Mars at ≈1 kg/s. More recent data taken during solar minimum by Mars Express, although with less adequate low-energy (<100 eV) coverage, implies a much lower outflow (<30 g, Barabash et al. 2007). The outflow rate also depends strongly on solar disturbances (solar EUV and solar wind dynamic pressure, Lundin et al. 2006b). The dominating escape flux based on Phobos-2 results comprise H^+, O^+, and $O_2^+ + CO_2^+$ (e.g. Lundin et al. 1989; Norberg et al. 1993). Recent Mars Express results (e.g. Carlsson et al. 2006) demonstrated that the escape flux constituted O^+ and O_2^+ in almost equal concentration, with a ≈10% admixture of CO_2^+. The predominant oxygen heavy ion escape is similar to that from the Earth (less the O_2^+ escape). This indicates a preference for the loss of water. CO_2 molecules disappear at a much slower rate despite the fact that the CO_2/H_2O content ratio in the atmosphere is about 1000. Dehydration therefore appears to be a most efficient process in accelerating and removing ionospheric ions, to the extent that it may even dominate the escape of water from arid planets like Mars. However, this does not preclude other processes from making substantial contribution to the escape such as e.g. photochemical escape and ion sputtering, for example (see Introduction and references therein).

The solar wind interaction with Mars and the corresponding energization and escape of ionospheric plasma, has been subject of theory and simulations for many years. The review

by Nagy et al. (2004) provides a good summary of the progress made in understanding the plasma environment of Mars based the Phobos-2 and Mars Global Surveyor (MGS) results. Figure 12a, based on Fig. 1.1 from Nagy et al. (2004), summarizes the insight gained in the analysis of data from Phobos-2 and MGS. Based on magnetic field data (Phobos-2, MGS), electron data (MGS) and 3 months of ion data (Phobos-2) the following features were identified:

1. The bow shock, which marks an obstacle to the solar wind expected from gas dynamics and/or magneto hydrodynamics. Inside the bow shock one finds shocked solar wind plasma, the magnetosheath.
2. The magnetic pileup Region, MPR, (Vignes et al. 2000), a region dominated by planetary ions. A Magnetic Pileup Boundary (MPB) separates MPR from the magnetosheath. MPB is a boundary that has had many names (see Nagy et al. 2004).
3. The ionosphere, separated to MPR by a boundary that resembles the Ionopause on Venus.

MPB, the boundary between the magnetosheath plasma and the plasma contained in the induced magnetosphere, has also been termed Induced Magnetosphere Boundary (IMB) (Lundin et al. 2004b). Moreover, the notion of the Photoelectron Boundary (PEB) has been introduced on the basis of Mars Express electron data (Lundin et al. 2004b) to mark the boundary separating the cold ionospheric plasma produced in the dayside and the hotter, induced magnetospheric plasma. PEB does not mark a strict boundary, though, because photoelectrons may reach high altitudes in the Martian tail (Frahm et al. 2006).

A review of modelling and simulations of the plasma environment of Mars is given by Nagy et al. (2004). Although in many aspects idealized, simulations provide an instantaneous global perspective of the plasma escape. Important progress has been made in understanding the ion-pickup process using, for instance, modern 3D hybrid models (e.g. Kallio and Janhunen 2002; Modolo et al. 2005) and 3D MHD fluid models (e.g. Ma et al. 2004; Harnett and Winglee 2005, and Luhmann et al. 2006).

Mars Express, launched in 2 June 2003, has provided a follow-up of the non-thermal escape from Mars. Results from the ion and electron analyzers of the ASPERA-3 experiment have considerably improved our understanding of solar forcing effects on Mars. For instance, Lundin et al. (2004b) noted that the solar wind penetrates deep into the dayside atmosphere, and may rapidly accelerate ions to high energies there. This implies that the entire dayside atmosphere of Mars is under intense solar wind forcing. The data also suggests a very corrugated contact surface between the ionosphere and the solar wind, in part due to the existence of patchy crustal magnetizations at Mars (Acuña et al. 1998) and the associated magnetic "cusps" (Krymskii et al. 2002). These "cusp/cleft" magnetic field lines are draped tailward (e.g. Harnett and Winglee 2005), promoting energization and outflow of ionospheric ions (Lundin et al. 2006b). The crustal magnetic field therefore acts as a stopper for incident solar wind plasma (closed field lines), as well as an acceleration region (Auroral Acceleration region, AA, Lundin et al. 2006c). Aside from the magnetic "anomalies", ion data from the flank and tail of Mars suggest many similarities between Mars and comets; the bulk of the flow following the external solar wind flow in the antisunward direction (e.g. Lundin and Dubinin 1992; Dubinin et al. 2006). A diagram summarizing the morphology of the ionospheric plasma outflow from Mars is illustrated in Fig. 12. AA stands for the Auroral Acceleration region in the tail. Except for pickup ions, most of the accelerated ionospheric ion outflow is contained inside IMB.

The composition of the ion outflow reflects the depth of solar forcing into the ionosphere. This is illustrated in Fig. 13, showing ASPERA-3 ion composition data (Lundin et al. 2006a)

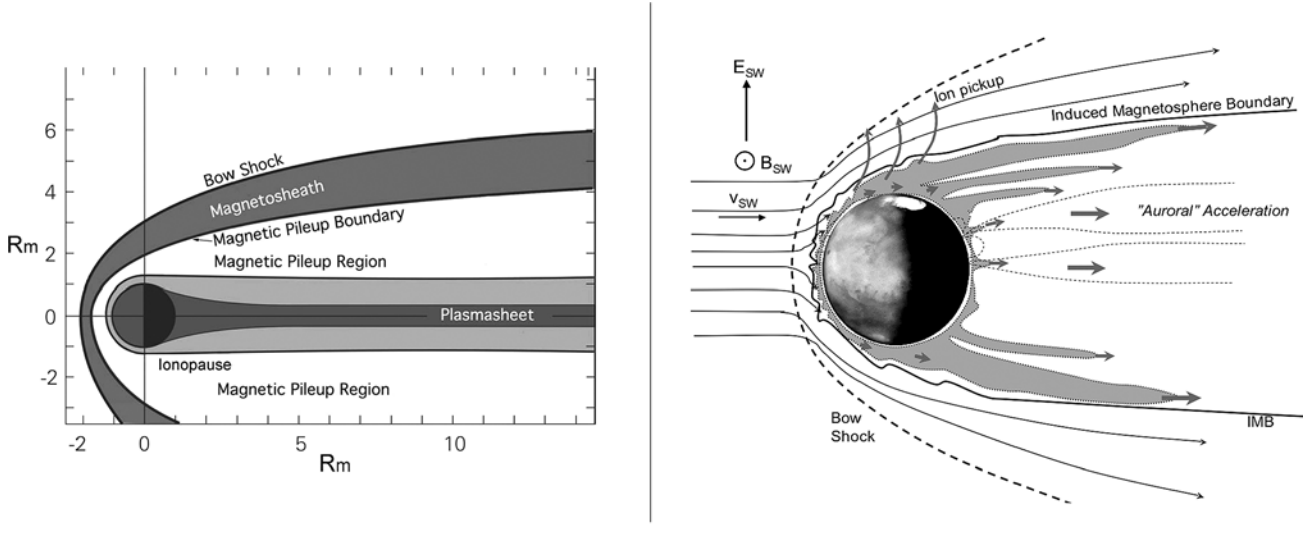

Fig. 12 Solar wind interaction with Mars. (**a**) (From Nagy et al. 2004) shows the structure of the Martian plasma environment based on primarily Phobos-2 and MGS results. (**b**) Demonstrates the energization and ionospheric plasma escape from Mars based on ion and electron measurements from Mars Express. Ion pickup (by the solar wind electric field) and ionospheric plasma energization (by waves and/or parallel electric fields) are illustrated schematically in (**b**)

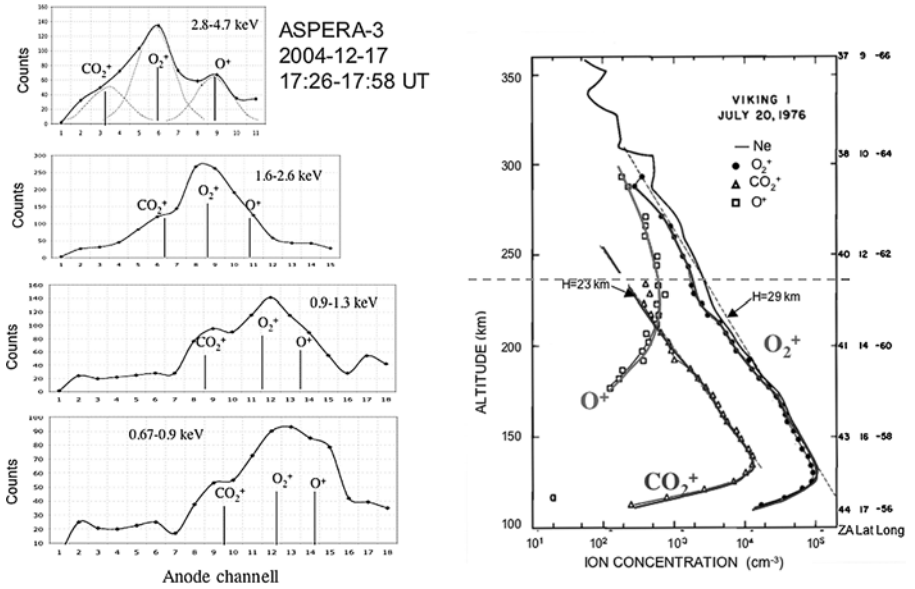

Fig. 13 *Left*: Ion mass spectra illustrating the composition of ionospheric outflow from Mars, with O_2^+ being most abundant, O^+ coming second and CO_2^+ coming third. The composition is similar to that observed by the Viking-1 spacecraft at an altitude of about 240 km (figure obtained from Hanson et al. 1977)

combined with an ionospheric density and an ion composition profile determined by the Viking-1 lander (Hanson et al. 1977). The accelerated ion composition of the outflow in 2004 is similar to the ionospheric composition in the altitude range 230–250 km as measured by Viking-1 in 1974, observations made 30 years apart but during the declining/minimum phase of solar activity. Figure 13 implies a somewhat higher CO_2^+/O^+ ratio than the average value of 8 found by Carlsson et al. (2006). However, the abundance ratios are quite variable, the ratio by Carlsson et al. (2006) marking an average. The CO_2^+/O^+ ratio may be interpreted as an altitude scalar for ion energization, a high ratio implying a low altitude for ion energization and vice versa.

Under the assumption that outflow of O^+ originates from water, the loss rate, acting over 4.5 billion years, Lundin et al. (1989) estimated the loss to a GEL of water of $\approx$1 m at Mars. This is certainly insufficient to explain a wetter early Mars (e.g. Carr and Head 2003). However, the 1 m estimate GEL of water level was based on constant solar forcing, and a constant supply. A wet early Mars also implies a dense atmosphere and grosser cross-sectional area (the outflow was higher in the past) leading to a higher total loss also for constant solar forcing. The Wood et al. (2002) findings about the evolution of sun-like stars, discussed in sections 2.3 and 2.4, have a major impact on solar forcing models. Based on these findings Lammer et al. (2003) estimated that Mars might have lost some 15–30 m GEL of water during the last 3.5 billion years. Considering also the impact of the early intense X-ray and EUV fluxes (Ribas et al. 2005) on the photochemistry and thermal properties of an early Martian atmosphere, the loss may have been even higher.

Assuming that all hydrogen lost to space from Mars originates from H_2O, theoretical studies and spacecraft observations indicate that the stoichiometrically H : O escape ratio of 2 : 1 to space cannot be maintained (Lammer et al. 2003; Patel et al. 2003). This result

implies an oxygen surface sink and a strong atmosphere-surface interaction. The oxygen surface sink, which is needed for establishing the 2 : 1 ratio between the H and O loss over the past 2 Gyr, may be responsible for enhanced soil/surface oxidation processes. Depending on different models of meteoritic gardening, the expected range for the oxidant extinction depth should be between 2–5 m. These constraints on the oxidant extinction depth are important for the search of organic material since in situ excavation of samples from the Martian subsurface.

5.3 Atmospheric Loss from Present Venus

Atmospheric escape from the upper atmosphere of Venus is mainly influenced by the loss of hydrogen and oxygen caused by the interaction of solar radiation and particle flux with the unmagnetized planetary environment. The loss of CO_2 and N_2 is estimated to be less significant, for reasons similar to those applicable for Mars (CO_2-loss) and the Earth (N_2-loss). The ionospheric ion composition altitude profile in Fig. 14 illustrates this quite well, the outflow replicating the ion abundance in the topside ionosphere.

Luhmann and Bauer (1992) presented a first estimate of the O^+ escape, $\approx 10^{25}$ s^{-1}($\approx$0.3 kg/s), based on Pioneer Venus Orbiter (PVO) ion data. Lammer et al. (2006) using a gas dynamic test particle model for average solar activity conditions deduced similar loss rates: 1×10^{25} s^{-1} and 1.6×10^{25} s^{-1}($\approx$0.4 kg/s) for H^+, and O^+ pick up ions, respectively. Estimations of ion loss rates due to detached plasma clouds that were observed by the Pioneer Venus Orbiter, yield O^+ ion loss rates in the order of about 10^{25} s^{-1} (Terada et al. 2002; Lammer et al. 2006). Due to the higher gravitational acceleration compared to Mars, thermal atmospheric escape and atmospheric loss by photo-chemically produced oxygen atoms yield negligible loss rates on Venus. Sputtering by incident pick up O^+ ions give O atom loss rates in the order of about 6×10^{24} s^{-1}. On the other hand, photo-chemically-produced, hot hydrogen atoms are a very efficient loss mechanism for hydrogen on Venus with a global average total loss rate of about 3–8 $\times 10^{25}$ s^{-1} (Donahue and Hartle 1992). This loss is of the same order as, but less than, the estimated H^+ ion outflow on the Venus nightside of about 7.0×10^{25} s^{-1} due to acceleration by an outward electric polarization force related to ionospheric holes (Hartle and Grebowsky 1993).

One finds that on Venus, due to its larger mass and size compared to Mars, the most relevant atmospheric escape processes of oxygen involve ions and are caused by the interaction with the solar wind and related processes. However, a detailed analysis of the outflow of ions from the Venus upper atmosphere by the ASPERA-4 and VEX-MAG instruments

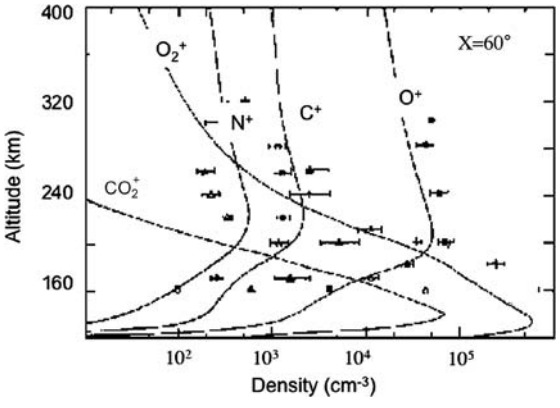

Fig. 14 Ion composition of the Venus ionosphere, illustrating the dominances of O_2^+ at low altitudes and O^+ atoms at high altitudes (after Nagy et al. 1980, and Hartle et al. 1980)

aboard ESA's Venus Express VEX will lead to more accurate atmospheric loss estimations and a better understanding of the planet's water inventory. New measurement results from 42 tail crossings with Venus Express (Lundin et al. 2007) suggest an even higher O^+ outflow (1.6×10^{26} s^{-1}), corresponding to a mass loss of 3.8 kg/s.

5.4 Amplified Particle Outflow

The evolution of the particle outflow from the Earth-like planets by solar forcing is a matter of time (solar evolution), internal properties (atmosphere, hydrosphere), and proximity to the Sun. The solar evolution as discussed in Sects. 2.2 and 2.3 implies very strong forcing in the early time period of the solar system. We now present a model of the planetary particle outflow based on solar mass losses (Wood et al. 2002, 2005) and solar EUV/XUV radiation (Ribas et al. 2005) versus time. The assumptions and boundary conditions are similar to those used in determining the theoretical outflow discussed in Sect. 3.4, incorporating the solar evolution and its effect on existing and past atmospheres of the Earth-like planets. We assume for the sake of simplicity that only the Earth had a protecting magnetic umbrella, while Venus and Mars remained essentially unmagnetized throughout. The model is fully analytical, starting with the presently measured/inferred planetary outflow and going back in time.

We start with the case of Mars, using as present outflow H^+, O^+, and O_2^+ ions (dissociated and ionized H_2O). Recent data from Mars Express indicates a highly solar EUV and solar wind dependent outflow, therefore also solar cycle dependent. The Phobos-2 data of 1 kg/s (solar maximum) is an order of magnitude higher than the MEX (solar minimum) values. We therefore assume an average escape flux of 0.5 kg/s from the present atmosphere, removed from a mean cross-sectional area $A_M \approx 1.6 \times 10^{14}$ (Sect. 3.4). The cross-sectional area is in effect an extension of the Martian atmosphere and ionosphere, specifically by the scale heights of H, O, and O_2, and the solar forcing (solar wind and EUV). Enhanced solar forcing leads to increased cross-sectional area and enhanced planetary outflow. This should apply forward as well as backward in time. From Wood et al. (2002, 2005) and Ribas et al. (2005) we obtain the following evolution of the solar mass loss/solar wind versus time.

$$\Phi_{SM}(t) \approx \Phi_0 t^{-\alpha_1}, \quad \alpha_1 \approx 1.8, \tag{3}$$

where $\Phi_{SM}(t)$ is the solar wind flux at a given time t and Φ_0 is the solar wind flux at 0.1 Gyr.

In a similar manner the following power-law relation is used for the decay of solar EUV radiation versus time:

$$\phi_{EUV}(t) \approx \phi_0 t^{-\alpha_2}, \quad \alpha_2 = 1.2. \tag{4}$$

The value for alpha is an approximation of the Ribas et al. (2005) and Lammer et al. (2003) value for the solar EVU decay ($\alpha_2 \approx 1.2$). Equation (4) implies a 98 times higher solar EUV flux at 0.1 Gyr than today (4.6 Gyr). These should be considered mean EUV flux values with time. In fact, the EUV flux values during a solar cycle ($\approx$11 years) may vary by a factor 2–4. This variability demonstrates the dynamic influence of the solar EUV/UV radiation on the planetary atmosphere and ionosphere.

The EUV radiation causes, besides ionization, heating and expansion of the Martian upper atmosphere and ionosphere and, consequently, an increased cross-section area for the solar wind interaction. Moreover, a higher atmospheric pressure for early Mars (0.3–0.5 bar, Kulikov et al. (2007), this issue) would further increase the solar wind interaction region.

Altogether, it seems reasonable to assume that the area, $A(t)$, also varies with time, i.e.

$$A(t) \approx A_M t^{-\alpha_2}, \quad \alpha_2 = 1.2, \tag{5}$$

where A_M is the area discussed in Sect. 3.4. Notice that the size of A_M is expected to scale with the atmospheric and ionospheric scale height. Atomic species (H^+, O^+) have larger scale heights, the interaction region extending much further into space compared to molecular species (O_2^+ and CO_2^+). In further analysis, we focus on the water-related heavy ions, O^+ and O_2^+, and consider in a very tentative way the escape of the main atmospheric constituent (CO_2^+). For O^+ we use the empirical value of the cross-sectional area (Sect. 3.4) $A_M = A_{O+}$. Considering the approximately factor of four larger scale height for CO_2^+ compared to O^+, (e.g. Hanson et al. 1977) the CO_2^+ area would scale as: $A_{CO_2^+} \approx A_{O^+}/16$. Furthermore, the sensitivity and thermal expansions from increased solar UV/EUV for CO_2 is low compared to that for O_2 and O. We here assume that the effective area for CO_2^+ scales with time as $A(t) \approx {A_{CO_2^+}}^{-\alpha_2}$, where $\alpha_2 = 0.6$.

We noted from (1) the connection between the mass-loaded escape flux from Mars (Φ_M) and the input solar wind flux (Φ_{SW}). The mass flux of the escaping ions will be substantially higher if the flow velocities are just a few times the escape velocity (≈5 km/s), as compared to the incident solar wind velocity (≈400 km/s) (Sect. 3.4, (1)). Nevertheless, we assume for the sake of simplicity that the incident solar wind mass flux results in an equivalent mass flux for the outflowing planetary wind. We also assume a relative momentum exchange thickness of 1 in (1).

Combining expressions (2) and (5) we now get the following species-dependent (M) expression describing the mass flux versus time escaping from Mars:

$$s_M(t) = m_M A_M(t) \Phi_M(t). \tag{6}$$

where m_M is the escaping ion mass, $A(t)$ is the cross-sectional area (species dependent) and $\Phi_M(t) = {\Phi_0}^{-\alpha_1}$ is the escape flux versus time. Inserting an average total escape rate (0.5 kg/s), with composition 45% O^+, 45% O_2^+, and 10% CO_2^+ (e.g. Carlsson et al. 2006) into expression (6) gives the time-dependent escape flux as depicted in Fig. 15. The cross-sectional size for O_2^+ is here scaled as $\alpha_2 = 0.9$, i.e. an intermediate value between O^+ and

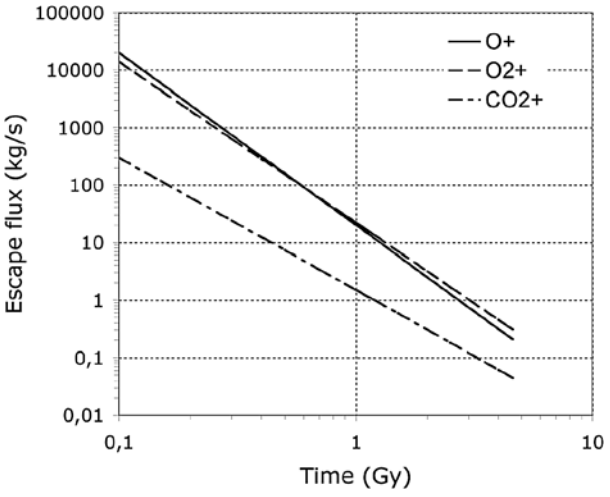

Fig. 15 Model describing the O^+, O_2^+, and CO_2^+ mass escape from Mars by solar forcing

CO_2^+. The much lower escape of CO_2^+ compared to O^+ and O_2^+, leads to atmospheric carbon enrichment. The selectivity of the process is best described by the fact that ≈10% of today's escape from Mars is carbon-based despite that ≈95% of the atmosphere is CO_2. 90% of the outflow originates from the mere 0.1% of water in the atmosphere. Recent VEX measurements indicate that the same applies for Venus, i.e. H^+ and O^+ dominates the ionospheric escape (Barabash et al. 2007).

A rather modest mass loss during the last ≈3 Gyr is expected from the model, the total inventory loss of O^+, O_2^+, and CO_2^+ corresponding to ≈0.1 Bar. The most critical time appears to be the first 500 million years. During that period the model predicts a loss corresponding to several tens of Bars. We emphasize that such a dramatic consequence of the model critically relies on the solar history (Wood et al. 2002, 2005 and Ribas et al. 2005). Nevertheless, if their findings are correct, it also implies that the early Noachian of Mars was wet, the early water inventory rapidly decreasing the first 1000 million years.

Notice that the above model of the volatile evolution on Mars is entirely based on solar EUV and particle forcing, addressing transport and photochemistry very qualitatively. We simply assume an upward atmospheric transport of water molecules capable of sustaining the 0.5 kg/s escape of H^+, O^+ and O_2^+. In view of the total atmospheric H_2O content ($\approx 10^{13}$ kg), this assumption is not unreasonable. Solar EUV and X-ray forcing is capable of providing sufficient thermal expansion, albeit following the solar variability. For reasons already discussed we also assume water to dominate the volatile loss process. Moreover, the model assumes that Mars lacked a sufficiently strong magnetic field to fend off the solar wind throughout its history. There is evidence for a magnetic dynamo acting on early Mars, but this dynamo may have ceased as early as 3.9–4.2 Gyr ago (e.g. Schubert et al. 2000). However, the solar forcing during this early period may have been so powerful that even a strong magnetic protection, such as that governed by the Earth's magnetic dynamo, may have been inadequate, leading to strong losses also from the Earth.

Based on the model one may also estimate the volatile loss from Earth and Venus. Venus resembles Mars in that it lacks a magnetic dynamo, let alone strong crustal magnetizations. The gravity is stronger; the CO_2 upper atmosphere is cooler, with a water-mixing ratio of $<10^{-5}$. Altogether, this leads to a less extended upper atmosphere/ionosphere and a reduced cross-sectional area for energy and momentum transfer by the solar wind. The first estimates of the ionospheric O^+ escape by Luhmann and Bauer (1992) indicated a tail loss of $\approx 10^{25}$ ions/s, corresponding to a mass escape rate of ≈0.3 kg/s. This should be regarded a lower limit since PVO lacked a mass resolving ion spectrometer, and O^+ ions were inferred from double peaks in ion energy spectra. Assuming ion pickup, the O^+ ions constitutes the high-energy peak (>1 keV) and H^+ ions the low-energy peak (≈1/16 of the O^+ peak). Recent measurements from VEX (Barabash et al. 2007) shows that large fluxes of O^+ ions escape at very low energies, the bulk outflow frequently peaking in the range 10–100 eV along the flanks of the Venus inner tail. Using ASPERA-4 ion data from 42 VEX tail traversals in August 2006 (over 1000 mass resolved ion spectra), and taking the average flux within a circular cross-sectional area of diameter $3R_V$, we obtain an average O^+ mass flux of 3.8 kg/s (Lundin et al. 2007). We use in the model as a conservative estimate 2 kg/s as the present average O^+ loss rate, assuming no magnetic shielding throughout the history of Venus, plus an expanding cross-sectional area (5) permanently exposed to the solar wind (3). Whereas we can use preliminary results for the O^+ loss rate in our model, we are still lacking an analysis of the CO_2^+ escape for Venus. We therefore use the same CO_2^+ percentage of the ion escape rate as for Mars (10% of total ion escape). This results in an accumulated CO_2-loss of ≈ 21% from 0.1 Byr up to now, barely visible on a logarithmic scale as in Fig. 16. This

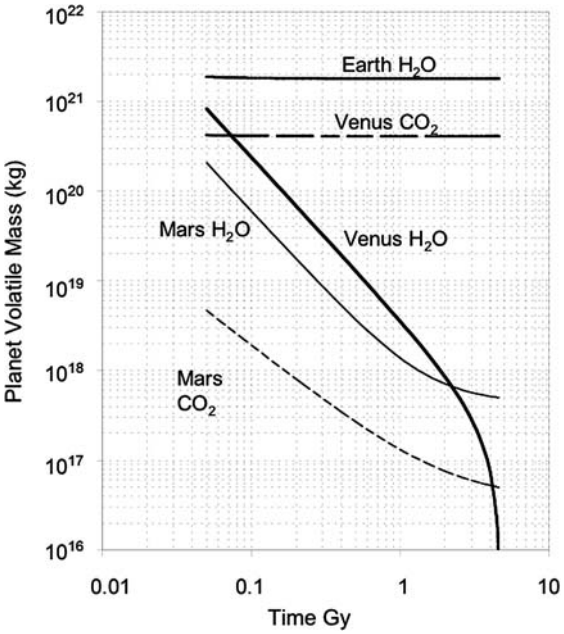

Fig. 16 Model describing the mass loss of H_2O and CO_2 on Venus, Earth and Mars by solar forcing. Strong magnetic shielding assumed for the Earth, no magnetic shielding for Venus, and options with and without magnetic shielding (up to 0.5 Gyr) for Mars. The H_2O inventory on the Earth remains essentially unaltered, while Mars and Venus have been subject to major losses

implies that if the CO_2^+ percentage ion escape is the same as for Mars the CO_2 inventory has changed only marginally by solar forcing throughout the lifetime of Venus.

Finally, the Earth's O^+ loss may be estimated based on the presently measured average loss rate of ≈1 kg/s. The total value may be even lower, considering the "recycling" back to the atmosphere (Seki et al. 2001). The Earth's atmosphere is also subject to an enhanced solar wind forcing (3) like for Venus and Mars. We assume for the sake of simplicity the same EUV forcing ($\alpha = 1.0$ in (5)) like that for Mars and Venus.

The total mass escaping from each of the Earth-like planets between a time t_0 (0.1 Gyr) and t_1 ($>t_0$) is obtained from the expression:

$$S_{\sum M t_1} = \sum_M \int_{t_0}^{t_1} s_M(t)\,\mathrm{d}t \text{ (kg)}. \tag{7}$$

The mass loss may be described as a decrease of the initial volatile inventory mass versus time. We focus here on water and CO_2, assuming that the escaping O^+ and O_2^+ ions originate from dissociated water. Adding the estimated water and CO_2 inventory described in Sect. 5 to the mass given by expression (7), we obtain the total inventory the history of water and CO_2 on the Earth-like planets as shown in Fig. 16. Notice that Earth and Venus have remained volatile-rich, albeit with predominantly water on the Earth and CO_2 on Venus. Mars has apparently lost most of its water and CO_2, but some still remains frozen in the polar cap deposits, for example. For Mars two curves are introduced regarding loss of water, with or without an Earth-like dipole magnetic field during the first 500 Myr. The magnetic protection is assumed to be as effective as the Earth's dipole field, illustrating that the water loss rate was substantial for Earth as well. Despite magnetic shielding on Mars the water loss is only reduced by about a factor of two during the first ≈500 Myr. The model implies that the young (0.1 Gyr) Earth-like planets had rather similar water and CO_2 inventories. However, Mars with its lower gravity and a smaller surface than

Earth and Venus had a correspondingly smaller inventory. Moreover, if the escape from Venus in the past was primarily H^+, O^+, and O_2^+, as for Mars (e.g. Norberg et al. 1993; Carlsson et al. 2006), Venus could have started with a GEL of water similar to that of the Earth (Kulikov et al. 2006). The lack of protection, and its proximity to the Sun, made most of the water disappear during the first billion years. The subsequent runaway greenhouse effect, governing a powerful hydrodynamic escape, would effectively remove any remaining hydrosphere on the surface of Venus.

6 Conclusions

The present difference in water and CO_2 inventories for Venus, Earth and Mars are substantial, water being the most abundant volatile on Earth, Venus dominated by a dense CO_2 atmosphere, and while Mars having a mix of water and CO_2, most of it supposedly as ice. "Why?", is a question still requiring a good answer. Most theories assume that a fierce early Sun (T-Tauri phase) removed all volatiles from the inner planets in the solar system, the volatiles subsequently restored by cometary impact. However, this requires a differentiated volatile insertion, with preference of water for the Earth. Another possibility is that a sufficiently high water and CO_2 inventory accumulated during the accretion phase, and a sufficiently strong gravity and magnetic shielding, may have been enough to retain an atmosphere and hydrosphere even after the early fierce phase of the Sun. If the latter is the case a secondary restoration of water and CO_2 is not necessary, and the present inventory of the Earth-like planets is the result of a long-term evolution. The water and CO_2 erosion model dating back in time to 0.1 Gyr after the planet formation, suggests that Earth, Venus and Mars may have had similar relative water and CO_2 inventories. Lacking magnetic shielding, Venus and Mars would have been more vulnerable than Earth, rapidly loosing the most abundant volatile molecule, water, by thermal and non-thermal escape. The model based on ionospheric plasma escape shows that non-thermal escape by solar forcing is sufficiently effective to remove some 40 Bar of water from Mars and at least 50 Bar of water from Venus. Similarly, the loss for Mars is consistent with estimates mentioned by Chassefière et al. (2007) and others. On the other hand, the model predicts that the loss of water from the Earth, a planet that retained its magnetic shielding, has been insignificant after 0.1 Gyr of the planet formation.

Notice that the loss of water and CO_2 may have been higher than presented here. A number of processes driven by solar forcing contribute to the escape of volatiles from the atmosphere of the Earth-like planets. Solar EUV/XUV forcing causes heating, expansion, and ionization of the atmosphere. Hydrodynamic escape (e.g. Chassefière 1996) is a process that may have been effective in the early removal of hydrogen. Photochemical escape (Nagy et al. 1980; Luhmann et al. 1992) due to dissociative recombination of heated ionospheric ions may have been effective in an early removal of oxygen. Solar wind forcing leads to further energization and escape of ionospheric plasma, but also to sputtering (Luhmann and Kozyra 1991). The latter results in the escape of neutrals. Altogether, there are good reasons to believe that solar forcing in the early solar system was capable of removing even more volatiles, specifically water, from Mars and Venus, than that implied from our model.

The ultimate fate for free/unbound atoms and molecules immersed in the inner solar system is to become picked up by the solar wind and brought to the solar system periphery. The solar wind interaction with a comet (Fig. 2) illustrates this quite well. The ionospheric

escape model presented here predicts a higher outflow for lower outflow velocity (expression (1) and Fig. 9). Compare for instance with the mass-loaded plasma outflow in the near tail of a comet, reaching velocities of 10–50 km/s. This velocity is an order of magnitude lower than the average solar wind velocity. With an early average solar wind velocity of ≈3000 km/s (Wood et al. 2005), and a correspondingly higher dynamic pressure (goes as square of the velocity) the amplification factor becomes substantially higher for the Earth-like planets. One may easily conceive a ten times higher mass loss than that perceived from the model.

In summary, we have presented important aspects of the long-term and short-term variability of solar forcing—solar X-ray EUV radiation and the solar wind. Solar forcing is expected to have played an important role in the atmospheric evolution of planets orbiting close to the Sun. We have here focussed on how solar forcing affects the ionosphere of the Earth-like planets; on a long-term perspective; with or without magnetic shielding. There should be no principle differences in physics governing the present short-term variability of ionospheric plasma escape from the Earth (e.g. Chappell et al. 1987; Yau and André 1997) and the long-term solar forcing effects on the atmosphere and ionosphere. The terrestrial escape flux may vary by an order of magnitude during a short duration (hours) solar disturbance (e.g. a CME). A similar trend, albeit much slower, is observed in the course of a solar cycle (≈11 years). If the findings by Wood et al. (2002, 2005) and Ribas et al. (2005) on the long-term variability of the Sun are correct it would imply a major differentiation of the volatile inventory of the Earth-like planets. Non-thermal escape acting in the early period of the solar system is capable of removing vast amounts of water on Mars and Venus. The first 500–1000 million years were probably the most critical period. Without sufficient magnetic shielding a planetary atmosphere would be subject to fierce solar forcing, effectively removing major fractions of the most volatile element—water. Unless being the only recipient of a vast additional water supply following the early solar forcing period the Earth must have endured the most dangerous period, thanks to a persistent intrinsic magnetic shield.

We conclude that a strong planetary dipole magnetic field has important implications for the evolution of life and for the habitability of a planet. A strong dipole magnetic field helps setting up a magnetic "umbrella", a stand off distance between the atmosphere and the eroding plasma wind from a star. Magnetic protection is particularly critical for planets near a young solar-like star during the first few hundred to one billion years. This is a period when solar-like stars irradiate planets with intense XUV/EUV and a fierce plasma wind. Without sufficient shielding this may lead to a climate crisis, with loss of water as major implication. Mars and Venus represent two extremes of the consequence of un-shielding, Mars a cold dehydrated planet with tenuous atmosphere, Venus a dehydrated planet with a hot dense atmosphere. Mars may have had a sufficiently dense atmosphere and water inventory the first billion years to qualify as "habitable" for primitive life forms. Also Venus is expected to have had a wealth of water during the first few hundred million years, potentially sufficient to qualify as "habitable" for at least primitive life forms. However, the first hundred million years of the Sun must have been an extremely harsh time for life. The solar variability a billion year later was more modest, with less implication on climate. With most of the hydrospheres on Venus and Mars gone, with a tenuous atmosphere on Mars and potentially already a runaway greenhouse on Venus, the habitability would anyway be at best marginal. Episodic habitability governed by solar and planetary conditions that changes climate in a favourable direction is a possibility. For instance, an atmospheric density and temperature above the triple point of water on Mars, combined with stable solar conditions, may

evolve into episodic habitability. Conversely, critical episodes with a combination of vanishing planetary magnetic protection and dramatically enhanced solar activity, may have had negative effects on a "favoured planet"—the Earth.

Acknowledgements R. Lundin acknowledges support from the Swedish National Space Board. H. Lammer and I. Ribas acknowledges support from the "Büro für Akademische Kooperation und Mobilität" of the Austrian Academic Exchange Service under the AD-Acciones Integradas project No. 12/2005. I. Ribas acknowledges also support from the Spanish Ministerio de Ciencia y Tecnologa through a Ramn y Cajal fellowship.

References

M.H. Acuña et al., Science **279**, 1676 (1998)
H. Alfvén, *Cosmical Electrodynamics* (Oxford University Press, Oxford, 1950)
T.R. Ayres, J. Geophys. Res. **102**, 1641–1651 (1997)
V.R. Baker, Nature **412**, 228–236 (2001)
S.J. Bauer, H. Lammer, *Planetary Aeronomy: Atmosphere Environments in Planetary Atmospheres* (Springer, Berlin, 2004)
S. Barabash, A. Fedorov, R. Lundin, J.-A. Sauvaud, Science (2007)
J.-P. Bibring, Y. Langevin, F. Poulet, A. Gendrin, B. Gondet, M. Berthé, A. Souflot, P. Drossart, M. Combes, G. Bellucci, V. Moroz, N. Mangold, B. Schmidt, OMEGA team, Nature **428**(6983), 627–630 (2004)
M.K. Bird, P. Edenhofer, in *Physics of the Inner Heliosphere I*, ed. by R. Schwenn, E. Marsch, vol. XI (Springer, Berlin, 1990), pp. 13–97
A. Bressan, F. Fagotto, G. Bertelli, C. Chiosi, Astron. Astrophys. Suppl. Ser. **100**, 647–664 (1993)
L.H. Brace, W.T. Kasprzak, H.A. Taylor, R.F. Theis, C.T. Russell, A. Barnes, J.D. Mihalov, D.M. Hunten, J. Geophys. Res. **92**, 15 (1987)
E. Carlsson et al., Icarus **182**(2), 320 (2006)
M.H. Carr, J.W. Head, J. Geophys. Res. **108**, 5042 (2003). doi:10.1029/2002JE001963
C.R. Chappell, T.E. Moore, J.H. Waite Jr, J. Geophys. Res. **92**, 5896 (1987)
E. Chassefière, Icarus **124**, 537–552 (1996)
E. Chassefière, F. Leblanc, Planet. Space Sci. **52**, 1039–1058 (2004)
E. Chassefière, F. Leblanc, B. Langlais, Planet. Space Sci. (2007). doi:10.1016/j.pss.2006.02.003
C.C. Chaston, L.M. Peticolas, C.W. Carlson, and 16 coauthors, J. Geophys. Res. **110**, A02211 (2005). doi:10.1029/2004JA010483
D.H. Crider, D.A. Brain, M.H. Acuña, D. Vignes, C. Mazelle, C. Bertucci, Space Sci. Rev. **111**, 203–221 (2004)
T.M. Donahue, R.E. Hartle, Geophys. Res. Lett. **19**, 2449–2452 (1992)
J.D. Dorren, E.F. Guinan, in *The Sun as a Variable Star*, ed. by J.M. Pap, C. Frolich, H.S. Hudson, S. Solanki (Cambridge Univ. Press, Cambridge, 1994), p. 206
E. Dubinin, R. Lundin, H. Koskinen, N. Pissarenko, J. Geophys. Res. **98**, 3991 (1993)
E. Dubinin, D. Winningham, M. Fränz, the ASSPERA-3 team, Icarus **182**(2), 343 (2006)
J.W. Dungey, Phys. Rev. Lett. **6**, 47–48 (1961)
J.R. Espley, P.A. Cloutier, D.H. Crider, D.A. Brain, M.H. Acuña, J. Geophys. Res. (2004). 2004AGUFMSA13A1120E
P. Foukal, C. Fröhlich, H. Spruit, T.M.L. Wigley, Nature **443**, 161–166 (2006). doi:10.1038
J.L. Fox, A. Hac, J. Geophys. Res. **102**, 24005–24011 (1997)
R.A. Frahm, J.R. Sharber, J.D. Winningham, the ASSPERA-3 team, Space Sci. Rev. **126**, 389–402 (2006)
E. Friis-Christensen, K. Lassen, Science **254**, 698 (1991)
B.F. Gordiets, Yu.N. Kulikov, M.N. Markov, M.Ya. Marov, J. Geophys. Res. **87**, 4504–4514 (1982)
J.-M. Griemeier, A. Stadelmann, T. Penz, H. Lammer, F. Selsis, I. Ribas, E.F. Guinan, U. Motschmann, H.-K. Biernat, W.W. Weiss, Astron. Astrophys. **425**, 753–762 (2004)
E.F. Guinan, I. Ribas, in *The Evolving Sun and its Influence on Planetary Environments*, ed. by B. Montesinos, A. Giménez, E.F. Guinan. ASP, vol. 269 (San Francisco, 2002), pp. 85–107
J.A. Guzik, L.S. Watson, A.N. Cox, Memorie della Societa Astronomica Italiana **77**, 389 (2006)
M. Güdel, E.F. Guinan, S.L. Skinner, Astrophys. J. **483**, 947–960 (1997)
E.M. Harnett, R.M. Winglee, J. Geophys. Res. **110** (2005). doi:10.1029/2003JA010315
W.B. Hanson, S. Sanatani, D.R. Zuccaro, J. Geophys. Res. **82**, 4351–4363 (1977)

R.E. Hartle, H.A. Taylor, S.J. Bauer, L.H. Brace, C.T. Russell, R.E. Daniell, J. Geophys. Res. **85**, 7739–7746 (1980)
R.E. Hartle, J.M. Grebowsky, J. Geophys. Res. **98**, 7437–7445 (1993)
D.V. Hoyt, K.H. Schatten, *The Role of the Sun in Climate Change* (Oxford University Press, Oxford, 1997)
D.E. Hunten, Science **259**, 915–920 (1993)
B.M. Jakosky, R.O. Pepin, R.E. Johnson, J.L. Fox, Icarus **111**, 271 (1994)
R.E. Johnson, D. Schnellenberger, M.C. Wong, J. Geophys. Res. **105**, 1659–1670 (2000)
E. Kallio, J.G. Luhmann, J.G. Lyon, J. Geophys. Res. **103**, 4753–4754 (1998)
E. Kallio, P. Janhunen, J. Geophys. Res. **107**(A3) (2002). doi:10.1029/2001JA000090
E. Kallio, A. Fedorovm, E. Budnik, the ASPERA-3 team, Icarus **182**(2), 448 (2006)
J. Kanipe, Nature **443**, 141–143 (2006)
J.F. Kasting, Icarus **74**, 472–494 (1988)
J.F. Kasting, D.P. Whitmire, R.T. Reynolds, Icarus **101**, 108–128 (1993)
R. Keppens, K.B. MacGregor, P. Charbonneau, Astron. Astrophys. **294**, 469–487 (1995)
J. Keyser, M.W. Dunlop, C.J. Owen, B.U.Ö. Sonnerup, S.E. Haaland, A. Vaivads, G. Paschmann, R. Lundin, L. Rezeau, Space Sci. Rev. **118**, 231–320 (2005)
J. Kim, A.F. Nagy, J.L. Fox, T. Craven, J. Geophys. Res. **103**(29), 29,339–29,342 (1998)
A.M. Krymskii, T.K. Breus, N.F. Ness, M.H. Acuña, J.E.P. Connerney, D.H. Crider, D.L. Mitchell, S.J. Bauer, J. Geophys. Res. **107**(A9), 1245 (2002). doi:10.1029/2001JA000239
Yu.N. Kulikov, H. Lammer, H.I.M. Lichtenegger, N. Terada, I. Ribas, C. Kolb, D. Langmayr, R. Lundin, E.F. Guinan, S. Barabash, H.K. Biernat, Planet. Space Sci. **54**, 1425–1444 (2006)
Yu.N. Kulikov, H. Lammer, H.I.M. Lichtenegger, T. Penz, D. Breuer, T. Spohn, R. Lundin, H.K. Biernat, Space Sci. Rev. (2007, this issue). doi: 10.1007/s11214-007-9192-4
H. Lammer, W. Stumptner, S.J. Bauer, Geophys. Res. Lett. **23**, 3353–3356 (1996)
H. Lammer, H.I.M. Lichtenegger, C. Kolb, I. Ribas, E.F. Guinan, R. Abart, S.J. Bauer, Icarus **106**, 9–25 (2003)
H. Lammer, H.I.M. Lichtenegger, H.K. Biernat, N.V. Erkaev, I.L. Arshukova, C. Kolb, H. Gunell, A. Lukyanov, M. Holmstrom, S. Barabash, T.L. Zhang, W. Baumjohann, Planet. Space Sci. (2006, in press)
J. Lean, Ann. Rev. Astron. Astrophys. **35**, 33–67 (1997)
F. Leblanc, R.E. Johnson, J. Geophys. Res. (2002). doi:10.1029/2000JE001473
J.S. Lewis, R.G. Prinn, *Planets and Their Atmospheres: Origin and Evolution* (Academic, Orlando, 1984)
J.G. Luhmann, J.U. Kozyra, J. Geophys. Res. **96**, 5457 (1991)
J.G. Luhmann, R.E. Johnson, M.H.G. Zhang, Geophys. Res. Lett. **19**, 2151 (1992)
J.G. Luhmann, S.J. Bauer, in *Venus and Mars: Atmospheres, Ionospheres, and Solar Wind Interactions*. AGU Monograph, vol. 66 (1992), pp. 417–430
J.G. Luhmann, S.A. Ledvina, J.G. Lyon, C.T. Russell, Planet. Space Sci. **54**, 1457–1471 (2006)
R. Lundin, A. Zakharov, R. Pellinen, B. Hultqvist, H. Borg, E.M. Dubinin, S. Barabasj, N. Pissarenko, H. Koskinen, I. Liede, Nature **341**, 609 (1989)
R. Lundin, E.M. Dubinin, S.V. Barabash, H. Koskinen, O. Norberg, N. Pissarenko, A.V. Zakharov, Geophys. Res. Lett. **18**, 1059 (1991)
R. Lundin, E.M. Dubinin, Adv. Space Res. **12**(9), 255 (1992)
R. Lundin, S. Barabash, Planet. Space Sci. **52**, 1059–1071 (2004a)
R. Lundin, S. Barabash, H. Andersson, M. Holmström, the ASPERA3 team, Science **305**, 1933 (2004b)
R. Lundin, D. Winningham, S. Barabash, R. Frahm, the ASPERA-3 team, Icarus **182**(2), 308 (2006a)
R. Lundin, S. Barabash, the ASPERA 3 team (2006b, manuscript under preparation)
R. Lundin, D. Winningham, S. Barabash, the ASPERA 3 team, Science **311**, 980–983 (2006c)
R. Lundin, S. Barabash, J.-A. Sauvaud, the ASPERA-4 team, Science (2007, submitted)
J.I. Lunine, J. Chambers, A. Morbidelli, L.A. Leshin, Icarus **165**, 1–8 (2003)
H. Lundstedt, L. Liszka, R. Lundin, R. Muschler, Annales Geophysicae **24**, 1–10 (2006)
M.B. McElroy, T.Y. Kong, Y.L. Yung, J. Geophys. Res. **82**, 4379–4388 (1977)
Y. Ma, A.F. Nagy, I.V. Sokolov, K.C. Hansen, J. Geophys. Res. **109**, A07211 (2004). doi:10.1029/2003JA010367
C.P. McKay, C.R. Stoker, Rev. Geophys. **27**, 189–214 (1989)
R. Modolo, G.M. Chanteur, E. Dubinin, A.P. Matthews, Ann. Geophys. **23**, 433–444 (2005)
T.E. Moore, R. Lundin, D. Alcayde, M. Andre, S.B. Ganguli, M. Temerin, A. Yau, Space Sci. Rev. **88** (1999)
A.F. Nagy, T.E. Cravens, S.G. Smith, H.A. Taylor, H.C. Brinton, J. Geophys. Res. **85**, 7795–7801 (1980)
A.F. Nagy, D. Winterhalter, K. Sauer et al., Space Sci. Rev. **111**(1), 33–114 (2004)
G. Neukum, New view of Mars after two years of Mars Express high resolution stereo camera data acquisition and analysis. American Geophysical Union, Fall Meeting 2005, abstract #P13C-03
G. Newkirk Jr., Geochimica Cosmochimica Acta Suppl. **13**, 293–301 (1980)
M.J. Newman, R.T. Rood, Science **198**, 1035–1037 (1977)

O. Norberg, R. Lundin, S. Barabash, in *COSPAR Colloquium 4, Plasma Environments of Non-magnetic Planets*, ed. by T.I. Gombosi (1993), pp. 299–304
T. Owen, in *Evolution of Planetary Atmospheres and Climatology of the Earth*. International Conference, Nice, France, A79-33839 13-42, Toulouse, CNRS, 1979, pp. 1–10
E.N. Parker, Astrophys. J. **128**, 664 (1958)
M.R. Patel, A. Berc¶es, C. Kolb, H. Lammer, P. Rettberg, J.C. Zarnecki, F. Selsis, Int. J. Astrobiol. **2**, 21–34 (2003)
R.O. Pepin, Icarus **111**, 289–304 (1994)
H. Pérez-de Tejada, J. Geophys. Res. **92**, 4713 (1987)
H. Pérez-de Tejada, J. Geophys. Res. **103**, 31499–31508 (1998)
I. Ribas, E.F. Guinan, M. Güdel, M. Audard, Astrophys. J. **622**, 680–694 (2005)
C.T. Russell, J.G. Luhmann, R.J. Strangeway, Planet. Space Sci. **54**, 1482–1495 (2006)
I.-J. Sackmann, A.I. Boothroyd, Astrophys. J. **583**, 1024–1039 (2003)
C. Sagan, G. Mullen, Science **177**, 52–56 (1972)
K. Seki, R.C. Elphic, M. Hirahara, T. Terasawa, T. Mukai, Science **291**, 1939–1941 (2001)
G. Schubert, C.T. Russell, W.B. Moore, Nature **408**, 666 (2000)
R. Schwenn, in *Large-Scale Structure of the Interplanetary Medium, Physics of the Inner Heliosphere I,* vol. XI, ed. by R. Schwenn, E. Marsch (Springer, Berlin, 1990), p. 99
T. Simon, E.F. Boesgaard, G. Herbig, Astrophys. J. **293**, 551–570 (1985)
A. Skumanich, Astrophys. J. **171**, 565–567 (1972)
H. Svensmark, E. Friis-Christensen, J. Atmosph. Sol.-Terr. Phys. **59**, 1225–1232 (1997)
H. Svensmark, Space Sci. Rev. **93**, 175–185 (2000)
H. Svensmark, J.O.P. Pedersen, N. Marsh, M. Enghoff, U. Uggerhøj, *Proceedings of the Royal Society A*, October 3rd, 2006
N. Terada, S. Machida, H. Shinagawa, J. Geophys. Res. **107**, 1471–1490 (2002)
D. Vignes, C. Mazelle, H. Rème, M.H. Acuña, J.E.P. Connerney, R.P. Lin, D.L. Mitchell, P. Cloutier, D.H. Crider, N.F. Ness, Geophys. Res. Lett. **27**(1), 49 (2000)
D.F. Webb, R.A. Howard, J. Geophys. Res. **99**, 4201–4220 (1994)
D.P. Whitmire, L.R. Doyle, R.T. Reynolds, J. Matese, J. Geophys. Res. **100**, 5457–5464 (1995)
J.D. Winningham, R.A. Frahm, J.R. Sharber, the ASPERA-3 team Icarus **182**(2), 360 (2006)
B.E. Wood, H.-R. Müller, G. Zank, J.L. Linsky, Astrophys. J. **574**, 412–425 (2002)
B.E. Wood, H.-R. Müller, G.P. Zank, J.L. Linsky, S. Redfield, Astrophys. J. **628**, L143–L146 (2005)
A.W. Yau, B.A. Whalen, Geophys. Res. Lett. **18**, 345–348 (1991)
A.W. Yau, B.A. Whalen, C. Goodenaough, E. Sagawa, T. Mukai, J. Geophys. Res. **98**, 11205–11224 (1993)
A.W. Yau, M. André, Space Sci. Rev. **37**, 1 (1997)
K.J. Zahnle, J.C.G. Walker, Rev. Geophys. **20**, 280–292 (1982)
T.L. Zhang, J.G. Luhmann, C.T. Russell, J. Geophys. Res. **96**, 11145 (1991)
M.H. Zhang, J. Luhmann, A.F. Nagy et al., J. Geophys. Res. **98**, 3311 (1993)
M.T. Zuber, D.E. Smith, S.C. Solomon, J.B. Abshire, R.S. Afzal et al., Science **282**, 2053–2060 (1988)